Magnon-microwave backaction noise evasion in cavity magnomechanics

V.A.S.V. Bittencourt,[1,*] C.A. Potts,[2,3,4] J. P. Davis,[5] and A. Metelmann[1,6,7]

[1] *ISIS (UMR 7006), Université de Strasbourg, 67000 Strasbourg, France*
[2] *Kavli Institute of NanoScience, Delft University of Technology, PO Box 5046, 2600 GA Delft, Netherlands*
[3] *Niels Bohr Institute, University of Copenhagen, Blegdamsvej 17, 2100 Copenhagen, Denmark*
[4] *Center for Hybrid Quantum Networks (Hy-Q), Niels Bohr Institute, University of Copenhagen, Copenhagen, Denmark*
[5] *Department of Physics, University of Alberta, Edmonton, Alberta T6G 2E9, Canada*
[6] *Institute for Theory of Condensed Matter, Karlsruhe Institute of Technology, 76131, Karlsruhe, Germany*
[7] *Institute for Quantum Materials and Technology, Karlsruhe Institute of Technology, 76344, Eggenstein-Leopoldshafen, Germany*

In cavity magnomechanical systems, magnetic excitations couple simultaneously with mechanical vibrations and microwaves, combining the tunability of the magnetization, the long lifetimes of mechanical modes and the whole measurement toolbox of microwave systems. Such hybrid systems have been proposed for applications ranging from thermometry to entanglement generation. However, backaction noise can hinder the measurement of the mechanical vibrations, potentially rendering such applications infeasible. In this paper, we investigate the noise introduced in a mechanical mode of a cavity magnomechanical system in a one-tone drive scheme and propose a scheme for realizing backaction evasion measurements of the mechanical vibrations. Our proposal consists of driving the microwave cavity with two tones separated by twice the phonon frequency and with amplitudes balanced to generate equal numbers of coherent magnons. We demonstrate that different configurations of such a scheme are possible and show that drives centered around the lower frequency magnon-microwave polariton in a triple resonance scheme add the minimum imprecision noise in the measurement, even though such configuration is not the most robust to imperfections.

I. INTRODUCTION

One of the most iconic features of quantum mechanics is the disturbance of a system due to measurements [1]. The random nature of quantum measurements performed in a system of interest via an apparatus implies the addition of measurement noise to the system to be probed [2], which can hinder applications such as sensing. Backaction evasion (BAE) schemes often rely on engineering a Hamiltonian, which is quantum non-demolition (QND) in an observable of the system to be measured. This means that the measurement of such an observable does not disturb its evolution. The price to be paid is strong noise contamination in non-commuting observables. Such engineered interaction can be realized in hybrid systems architecture, a prominent example being the BAE scheme for measuring mechanical vibration in optomechanical systems [3–8]. Other examples include electromechanical systems [9–11], atomic ensembles coupled to mechanical resonators [12], Bose-Einstein condensates [13], and superconducting qubits coupled to microwave cavities [14].

Cavity magnomechanical systems have recently emerged as a promising platform for quantum technologies [15, 16]. In such systems, a magnetic element, usually made of yttrium iron garnet, is loaded into a microwave cavity, as we depict in Fig. 1. The magnetic excitation (magnons) couple simultaneously to the microwaves (via magnetic dipole coupling) and to the elastic vibrations of the material (via magnetoelastic effects) [15, 17–19]. Such a system allows the drive and measurement of phonons via the microwave resonator while retaining the tunability of the magnons. Among the potential applications proposed for such systems are the generation of entangled states [20–22], the generation of squeezing of magnons and phonons via magnon nonlinearities [23, 24], noise-based thermometry [25] and microwave-to-optical frequency conversion [26].

Due to a frequency mismatch, the coupling between magnons and phonons in cavity magnomechanical systems resembles that of an optomechanical system [15, 19]. Consequently, the mechanical oscillator experiences *dynamical backaction* [15, 27], namely, a frequency shift and modified decay due to its interaction with the magnons. Different from its optomechanical counterpart, magnons hybridize with microwaves, changing some characteristics of dynamical backaction. Recently, it was experimentally shown [28] that (classical) dynamical backaction can be evaded in such systems by judiciously choosing the microwave drive frequency. Nevertheless, up to date, there is no (quantum) BAE scheme tailored for cavity magnomechanical systems, a feature that could allow further applications of such systems at the quantum level, for instance, the measurement of entangled states that can be engineered in such systems [20, 29].

In this paper, we propose a scheme for evading quantum backaction in a cavity magnomechanical system. We first characterize the magnomechanical noise introduced in the phonon mode in a one-tone

* sant@unistra.fr

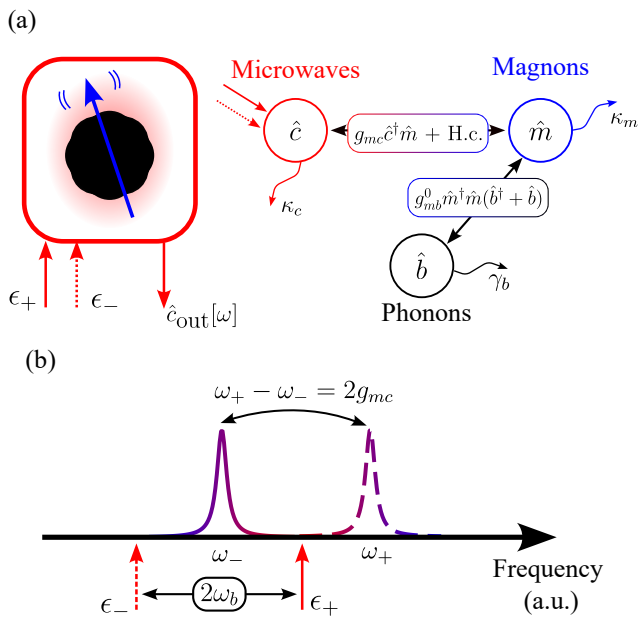

FIG. 1. (a) Schematic depiction of a cavity magnomechanical system: magnetic excitations (blue) couple simultaneously to a microwave mode (red) and mechanical vibrations (black). The cavity can be driven and the output is used to probe the mechanics. The system is described by a model of interacting bosonic modes subject to dissipation. (b) The two-tone driving scheme that yields a backaction evasion measurement of the mechanics. Magnons and microwaves form hybrid modes with frequencies $\omega_\pm$. The two drives $\epsilon_\pm$ must be separated by twice the phonon frequency ω_b. Centering the tones around the lower hybrid mode frequency yields the minimum added noise in the measurement of the mechanics.

setup, in correspondence with the recent experiments in which *dynamical backaction* is evaded. We then propose a scheme inspired by BAE schemes in opto and electromechanics [3, 4, 9] in which a two-tone drive applied to the microwave cavity realizes a QND Hamiltonian for a phonon quadrature. Our scheme requires that the tone frequencies are separated by twice the phonon frequency, as shown in Fig. 1(b), and the amplitudes of the drives have to be balanced to generate the same number of coherent magnons. The tone frequency separation provides a modulation of the magnomechanical force, which in turn yields a quantum non-demolition Hamiltonian involving one quadrature of the phonon mode [1]. We study the robustness of the system to imperfections of the parameters and quantify the noise added to the measurement of the mechanics. We show that for drives centered around the hybrid magnon-microwave modes frequency, the imprecision noise can go below the standard quantum limit. The drawback is that the BAE is less robust to imperfections, for example, slight deviations in the drive frequencies, for such configurations. Two-tone drive schemes have been proposed for magnomechanical systems to generate squeezing [30, 31] and induce magnonic frequency combs [32], and our scheme might allow future applications of cavity magnomechanical systems that rely on quantum features of the phonon mode.

This paper is structured as follows. In Section II we present a brief description of a cavity magnomechanical Hamiltonian, and calculate the backaction noise acting on a quadrature of the phonon mode for a single tone drive. We show in this section that the dynamical backaction evasion point demonstrated in [28] does not correspond to a quantum BAE point. In Section III we present our BAE scheme, and quantify the noise that acts on the quadrature conjugated to the BAE quadrature. In section IV, we compute the imprecision noise added to the measurement of the BAE quadrature via the output of the microwave mode. Finally, we present our conclusions and outline of the work in section V. We present full formulas and some detailed derivations in the appendix.

II. CAVITY MAGNOMECHANICS HAMILTONIAN AND MAGNOMECHANICAL BACKACTION NOISE

The cavity magnomechanical system depicted in Fig. 1 can be modelled with the following Hamiltonian [15, 19, 33]

$$\begin{aligned}\frac{\hat{H}}{\hbar} &= \omega_c\hat{c}^\dagger\hat{c} + \omega_m\hat{m}^\dagger\hat{m} + \omega_b\hat{b}^\dagger\hat{b} \\ &+ g_{mc}\left(\hat{m}^\dagger\hat{c} + \hat{m}\hat{c}^\dagger\right) + g^0_{mb}\hat{m}^\dagger\hat{m}\left(\hat{b}^\dagger + \hat{b}\right) \\ &+ \frac{\hat{H}_{\rm drive}}{\hbar}.\end{aligned} \tag{1}$$

A microwave mode $\hat{c}$ with frequency ω_c couples to a magnon mode $\hat{m}$ with frequency ω_m, which in turn couples to a phonon mode $\hat{b}$ with frequency ω_b. The magnon frequency ω_m can be tuned by an applied external field [34]. Magnons and microwaves couple via magnetic dipole interaction, and in the limit of a magnet with a volume smaller than the effective microwave mode volume, the corresponding coupling rate between the uniform magnon mode and a microwave mode g_{mc} depends on the intensity of the magnetic field at the magnet's positions and on the magnet volume V_m [35, 36]. Magnons and phonons, on the other hand, couple via magnetoelastic effects [37], and the Hamiltonian describing the interaction depends on the geometry of the magnet and the relative frequency between the magnon modes and the phonon modes [19]. Hereafter, we consider exclusively the case in which the uniform magnon mode, the Kittel mode, couples with a low-frequency phonon mode [15, 27, 28]. The single-magnon magnomechanical coupling g^0_{mb} depends on an overlap integral, which in general scales with $1/\sqrt{V_m}$ [19, 33]. A more detailed discussion and derivation of the coupling rates $g_{mb,mc}$ can be found in [19, 33]. The last term of the Hamiltonian

describes the microwave drive, which, for now, we assume to be a single-tone coherent drive

$$\frac{\hat{H}_{\rm drive}}{\hbar} = i\sqrt{\kappa_e}\epsilon_D(\hat{c}e^{i\omega_d t} - \hat{c}^\dagger e^{-i\omega_d t}), \tag{2}$$

with frequency ω_D and amplitude $\epsilon_D = \sqrt{\mathcal{P}/\hbar\omega_d}$.

The open dynamics of the system is described by the set of Heisenberg-Langevin equations

$$\begin{aligned}
\dot{\hat{c}} &= \left(-i\omega_c - \frac{\kappa_c}{2}\right)\hat{c} - ig_{mc}\hat{m} - \sqrt{\kappa_e}\epsilon_D e^{i\omega_d t} \\
&\quad + \sqrt{\kappa_c}\hat{c}_{\rm in}(t), \\
\dot{\hat{m}} &= \left(-i\omega_m - \frac{\kappa_m}{2}\right)\hat{m} - ig_{mc}\hat{c} \\
&\quad - ig^0_{mb}\hat{m}\left(\hat{b} + \hat{b}^\dagger\right) + \sqrt{\kappa_m}\hat{m}_{\rm In}(t), \\
\dot{\hat{b}} &= -\left(i\omega_b + \frac{\gamma_b}{2}\right)\hat{b} - ig^0_{mb}\hat{m}^\dagger\hat{m} + \sqrt{\gamma_b}\hat{b}_{\rm In}(t),
\end{aligned} \tag{3}$$

where $\{\kappa_c, \kappa_m, \gamma_b\}$ are the microwave, magnon and phonon linewidths respectively. The operators $\hat{c}_{\rm In}$, $\hat{m}_{\rm In}$, $\hat{b}_{\rm In}$ describe the noise acting in each mode. Typically, microwave noise includes both intrinsic thermal noise and noise from the input drive, while the magnon and phonon noises are entirely thermal. The microwave-magnon coupling can be stronger than both microwave and magnon decay rates, generating a hybridization between the modes [35, 38, 39]. In such a regime, two magnon-microwave polaritons form at frequencies $\omega_\pm$. We call the mode with frequency $\omega_+ > \omega_-$ the upper hybrid mode while the other is the lower hybrid mode. In the case where the magnon mode is resonant with the microwave mode $\omega_m = \omega_c$, the difference between the hybrid modes frequencies is $\sim 2g_{mc}$. Throughout the paper, we will consider exclusively the situation in which magnons and microwaves are at resonance, corresponding to maximum hybridization between the modes.

We consider parameters corresponding to experiments in which a 3D microwave cavity is loaded with a YIG sphere with radius $\sim 100\,\mu$m. In this case, the magnon and microwave frequencies are in the $\sim$ 10 GHz range, while their decay is typically a few MHz. Typically, $g_{mc} \sim 10$ MHz, with the possibility of reaching stronger couplings by tuning the cavity design [35, 38, 39]. We consider phonon modes corresponding to elastic vibrations of the sphere with frequencies in the 10 MHz range, such as spherical modes [40]. The linewidths of such modes depend on the specific design of the system. In the first experiments [15], the magnetic sphere was glued to a post, yielding higher phonon linewidths, while in [27] the sphere was free to move inside a capillary, for which the elastic vibrations exhibit higher quality factors. Here, we consider the first situation, for which $\gamma_b \sim$ kHz. The parameters used in the paper are summarized in table I. The chosen drive amplitude ϵ_D corresponds to a power $\sim$ 0.3 mW, which ensures a substantial enhancement of the magnomechanical coupling while keeping the system far from any unstable points [15, 27].

To characterize the quantum noise driving the phonon mode in a magnomechanical system, we linearize the Hamiltonian in Eq. (1), which in a frame rotating at the drive frequency ω_d reads

$$\begin{aligned}
\frac{\hat{H}_L}{\hbar} &= -\Delta_c\hat{c}^\dagger\hat{c} - \tilde{\Delta}_m\hat{m}^\dagger\hat{m} + \Omega_b\hat{b}^\dagger\hat{b} + g_{mc}(\hat{m}^\dagger\hat{c} + \hat{m}\hat{c}^\dagger) \\
&\quad + (g^*_{mb}\hat{m} + g_{mb}\hat{m}^\dagger)(\hat{b}^\dagger + \hat{b}),
\end{aligned} \tag{4}$$

where $g_{mb} = g^0_{mb}\bar{m}$, with $\bar{m}$ the coherent steady-state magnon amplitude given by

$$\bar{m} = \frac{ig_{mc}\sqrt{\kappa_e}\epsilon_D}{\left(i\Delta_c - \frac{\kappa_c}{2}\right)\left(i\Delta_m - \frac{\kappa_m}{2}\right) + g^2_{mc}}. \tag{5}$$

The linearization procedure was discussed in detail, for example, in [25, 27, 33]. The dynamics of the fluctuations $\hat{c}$, $\hat{m}$ and $\hat{b}$ can be described by a set of linear Heisenberg-Langevin equations, which in the frequency domain are given by [41]

$$\begin{aligned}
\chi_c^{-1}[\omega]\hat{c}[\omega] &= -ig_{mc}\hat{m}[\omega] + \sqrt{\kappa_c}\hat{\xi}_c[\omega], \\
\chi_m^{-1}[\omega]\hat{m}[\omega] &= -ig_{mb}(\hat{b}[\omega] + \hat{b}^\dagger[\omega]) \\
&\quad - ig_{mc}\hat{c}[\omega] + \sqrt{\kappa_m}\hat{\xi}_m[\omega], \\
\chi_b^{-1}[\omega]\hat{b}[\omega] &= -i(g^*_{mb}\hat{m}[\omega] + g_{mb}\hat{m}^\dagger[\omega]) \\
&\quad + \sqrt{\gamma_b}\hat{\xi}_b[\omega],
\end{aligned} \tag{6}$$

where the susceptibilities are

$$\begin{aligned}
\chi_{c,m}[\omega] &= \frac{1}{-i(\omega + \Delta_{c,m}) + \kappa_{c,m}/2}, \\
\chi_b[\omega] &= \frac{1}{-i(\omega - \omega_b) + \gamma_b/2},
\end{aligned} \tag{7}$$

and in what follows, we consider exclusively thermal noise for the fluctuations, such that

$$\begin{aligned}
\langle\hat{\xi}_i[\omega]\hat{\xi}_i[\omega']\rangle &= \langle\hat{\xi}^\dagger_i[\omega]\hat{\xi}^\dagger_i[\omega']\rangle = 0, \\
\langle\hat{\xi}^\dagger_i[\omega]\hat{\xi}_i[\omega']\rangle &= 2\pi n_i\delta(\omega + \omega'), \\
\langle\hat{\xi}_i[\omega]\hat{\xi}^\dagger_i[\omega']\rangle &= 2\pi(n_i + 1)\delta(\omega + \omega'),
\end{aligned} \tag{8}$$

where $n_{c,m,b}$ are the thermal occupancies of the respective baths. The equations (6) can be solved for $\hat{b}[\omega]$ giving

$$\tilde{\chi}_b^{-1}[\omega]\hat{b}[\omega] = -i\hat{f}_{\rm BA}[\omega] + \sqrt{\gamma_b}\hat{\xi}_b[\omega] + i\Sigma_b[\omega]\hat{b}^\dagger[\omega]. \tag{9}$$

The last term of the above equation is a counter-rotating term that we will discard. We assess the effects of this term in the appendix.

The magnomechanical coupling has two main implications for the phonon dynamics in such a linear framework. First, the phonon susceptibility $\chi_b[\omega]$ is modified to $\tilde{\chi}_b[\omega]$, corresponding to a *dynamical backaction* change of the phonon frequency and linewidth. Such an effect can be exploited, for instance,

TABLE I. Typical parameters of a cavity magnomechanical system consisting of a magnetic sphere loaded in a 3D microwave cavity, as described by the Hamiltonian in Eq. (1) and the Heisenberg-Langevin equations Eqs. (3).

Parameter	**Symbol**	**Value**
Microwave mode frequency	ω_c	$2\pi \times 10$ GHz
Magnon mode frequency	ω_m	$\sim \omega_c$ (tunable)
Phonon mode frequency	ω_b	$10^{-3}\omega_c$
Microwave intrinsic decay rate	κ_c	$2 \times 10^{-4}\omega_c$
Magnon mode decay rate	κ_m	$10^{-4}\omega_c$
Phonon intrinsic decay rate	γ_b	$10^{-7}\omega_c$
Magnon-microwave coupling rate	g_{mc}	$\sim 10^{-3}\omega_c$ (different cases will be considered)
Magnomechanical vacuum coupling rate	$g_{mb}^{(0)}$	$10^{-12}\omega_c$
Microwave drive amplitude	ϵ_D	$2.8 \times 10^4 \omega_c^{1/2}$

to cool down or amplify the mechanics depending on the drive detuning. The effective phonon susceptibility is given explicitly by

$$\tilde{\chi}_b^{-1}[\omega] = \chi_b^{-1}[\omega] - i\Sigma_b[\omega], \tag{10}$$

where the phonon self-energy $\Sigma_b[\omega]$ reads

$$\Sigma_b[\omega] = i|g_{mb}|^2 \left(\Xi_m[\omega] - \Xi_m^*[-\omega]\right), \tag{11}$$

which in turn is given in terms of the modified magnon susceptibility

$$\Xi_m^{-1}[\omega] = \chi_m^{-1}[\omega] + g_{mc}^2\chi_c[\omega]. \tag{12}$$

The effective mechanical susceptibility can be written as

$$\tilde{\chi}_b^{-1}[\omega] = -i(\omega - \tilde{\omega}_b) + \frac{\tilde{\gamma}_b}{2}, \tag{13}$$

where the effective frequency and linewidths are

$$\begin{aligned} \tilde{\omega}_b &= \omega_b - \mathrm{Re}[\Sigma_b[\omega]], \\ \tilde{\gamma}_b &= \gamma_b + 2\mathrm{Im}[\Sigma_b[\omega]] \end{aligned} \tag{14}$$

Dynamical backaction effects have been theoretically and experimentally explored in cavity magnomechanics in Refs. [15, 25, 27, 28, 33]. Second, the magnomechanical coupling drives the phonon mode with the backaction noise term $\hat{f}_{\mathrm{BA}}[\omega]$ given explicitly by

$$\hat{f}_{\mathrm{BA}}[\omega] = g_{mb}^*\hat{\xi}_{\mathrm{BA}}[\omega] + g_{mb}\hat{\xi}_{\mathrm{BA}}^\dagger[\omega], \tag{15}$$

where

$$\hat{\xi}_{\mathrm{BA}}[\omega] = \Xi_m[\omega](\sqrt{\kappa_m}\hat{\xi}_m[\omega] - ig_{mc}\sqrt{\kappa_c}\chi_c[\omega]\hat{\xi}_c[\omega]). \tag{16}$$

Dynamical backaction can be evaded by a careful choice of the drive frequency. In fact, for magnons at resonance with microwaves ($\omega_m = \omega_c$) one can show that $\Sigma_b[\omega] = 0$ for a drive on resonance with the microwave mode, i.e., $\Delta_{c,m} = 0$. This can also be understood as a balance between Stokes and anti-Stokes scattering processes from the magnon-microwave hybrid modes [28]. Such a dynamical backaction evasion was recently demonstrated in [28]. In contrast, backaction noise does not necessarily vanish, thus even if the phonon mode has no modification in its damping due to the magnomechanical coupling, the backaction noise $\hat{f}_{\mathrm{BA}}$ can still drive the mechanical motion in addition to the thermal noise described by $\hat{\xi}_b$. To quantify such an effect, we consider the mechanical noise spectral density [2]

$$S_{xx}[\omega] = \int_{-\infty}^{\infty} \frac{d\omega'}{2\pi} \langle \hat{x}_b[\omega]\hat{x}_b[\omega'] \rangle, \tag{17}$$

where

$$\hat{x}_b[\omega] = \frac{\hat{b}[\omega] + \hat{b}^\dagger[\omega]}{\sqrt{2}}. \tag{18}$$

$S_{xx}[\omega]$, which for brevity we call simply the noise spectrum, has units of inverse frequency and gives the position noise spectrum of the mechanical vibration via $x_{\mathrm{ZPF}}^2 S_{xx}[\omega]$, where x_{ZPF} are the zero-point fluctuations of the phonon mode. For a magnomechanical system, x_{ZPF} depends on the elastic coefficients of the material as well as the particular mode profile of the elastic vibrations [33]. The noise spectrum S_{xx} quantifies the ability of the mechanical oscillator to absorb and emit phonons into its environment [5]. In fact, for an oscillator in thermal equilibrium

$$S_{xx}^{(0)}[\omega] = \gamma_b \left[(n_b + 1)|\chi_b[\omega]|^2 + n_b|\chi_b[-\omega]|^2\right]. \tag{19}$$

The integral of the noise spectrum, which we indicate by I_{xx}, gives the expectation value $\langle \hat{x}^2 \rangle$. For an oscillator in thermal equilibrium, it reads [5]

$$I_{xx}^{(0)} \equiv \int_{-\infty}^{\infty} \frac{d\omega}{2\pi} S_{xx}^{(0)}[\omega] = \langle \hat{x}^2 \rangle = n_b + \frac{1}{2}. \tag{20}$$

Another important quantity to be discussed throughout the paper is the *symmetrized* noise spectrum

$$\begin{aligned} \bar{S}_{xx}^{(0)}[\omega] &= \frac{S_{xx}^{(0)}[\omega] + S_{xx}^{(0)}[-\omega]}{2} \\ &= \gamma_b \left(n_b + \frac{1}{2}\right) \left(|\chi_b[\omega]|^2 + |\chi_b[-\omega]|^2\right). \end{aligned} \tag{21}$$

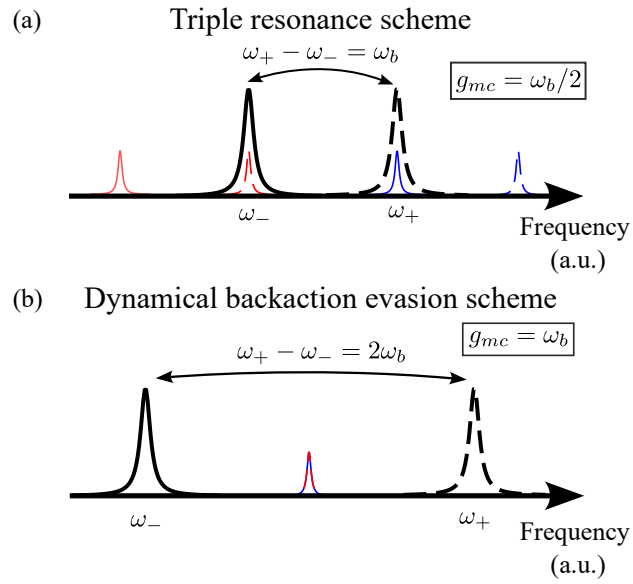

FIG. 2. Different cavity magnomechanics schemes. The lorentzians indicate the resonance frequency and linewidths of the hybrid modes as they would be measured, e.g. via transmission. Relevant mechanical sidebands are indicated as small lorentzians (a) Triple resonance scheme: the magnon-microwave coupling g_{mc} is half of the phonon frequency. The blue (red) sideband of the lower (upper) hybrid mode coincides with the upper (lower) hybrid mode frequency. (b) Dynamical backaction evasion scheme: the magnon-microwave coupling is equal to one phonon frequency. In this scheme, the sidebands of the hybrid modes coincide.

Specifically, at zero temperature and for a high-quality factor oscillator $\omega_b \gg \gamma_b$

$$\bar{S}^{(0)}_{xx}[\omega_b] = \frac{2}{\gamma_b}. \tag{22}$$

The backaction noise $\hat{f}_{\rm BA}$ drives the phonon mode and modifies its noise spectral density. In fact, from Eq. (9) we obtain

$$S_{xx}[\omega] = S^{(\rm D)}_{xx}[\omega] + S^{(\rm BA)}_{xx}[\omega]. \tag{23}$$

The first term in Eq. (23) reads

$$S^{(\rm D)}_{xx}[\omega] = \gamma_b \left[(n_b+1)|\tilde{\chi}_b[\omega]|^2 + n_b|\tilde{\chi}_b[-\omega]|^2\right], \tag{24}$$

which has a form similar to the uncoupled noise spectral density $S^{(0)}_{xx}$ but with the modified susceptibility $\tilde{\chi}_b$. Such a term includes only the dynamical backaction modifications of the phonon linewidth and frequency. The term $S^{(\rm BA)}_{xx}[\omega]$ is the backaction noise contribution due to the magnon-microwave hybrid modes driving the phonon quadrature x, and it is given by

$$\begin{aligned} S^{(\rm BA)}_{xx}[\omega] = \kappa_c g^2_{mc}|g_{mb}\mathcal{F}_{\rm BA}[\omega]|^2|\chi_c[\omega]|^2\Big[&|\Xi_m[-\omega]|^2 n_c \\ &+ |\Xi_m[\omega]|^2(n_c+1)\Big] \\ &+ \gamma_m|g_{mb}\mathcal{F}_{\rm BA}[\omega]|^2\Big[|\Xi_m[-\omega]|^2 n_m \\ &+ |\Xi_m[\omega]|^2(n_m+1)\Big], \end{aligned} \tag{25}$$

where

$$\mathcal{F}_{\rm BA}[\omega] = \tilde{\chi}_b[\omega] - \tilde{\chi}^*_b[-\omega]. \tag{26}$$

Both dynamical backaction and the backaction noise driving the mechanics modify $\langle \hat{x}^2 \rangle$.

We quantify the effects of the backaction noise by comparing the symmetrized noise spectrum $\bar{S}_{xx}[\omega]$ with Eq. (21). Specifically, we consider two experimentally relevant cavity magnomechanics driving schemes. The first one is for a separation of the hybrid modes matching the phonon frequency, realized by setting $g_{mc} = \omega_b/2$. In this case, the blue mechanical side-band of the lower hybrid mode coincides with the higher hybrid mode frequency, allowing the tune of a triple resonance condition: scattering between the hybrid modes via a phonon becomes very efficient. This regime was explored, for instance, in [27] and can be used to heat (amplify) or cool (damp) the phonon mode via dynamical backaction. The second scheme is obtained by setting $g_{mc} = \omega_b$, such that the blue mechanical side-band of the lower hybrid mode coincides with the red mechanical side-band of the higher hybrid mode. In this case, it is possible to balance scattering to and from both hybrid modes by tuning the drive detuning, allowing dynamical backaction to be evaded, as experimentally demonstrated in [28]. We call this scheme the dynamical backaction evasion scheme. We depict both schemes in Fig. 2.

We show in Fig. 3a comparison between the noise spectrum for the triple resonance and the dynamical backaction schemes for red and blue detunings, $\Delta_c = -g_{mc}$, and g_{mc}. At the phonon frequency, the symmetrized noise spectrum, for $\omega_b \gg \gamma_b$, reads

$$\bar{S}_{xx}[\omega_b] = \bar{S}^{(0)}_{xx}[\omega_b]\frac{\gamma_b}{\tilde{\gamma}_b} + \bar{S}^{(\rm BA)}_{xx}[\omega_b], \tag{27}$$

and if the parameter regime is such that $\gamma_b < \tilde{\gamma}_b$, i.e., if dynamical backaction increases the phonon linewidth (magnomechanical cooling), it is possible that $\bar{S}_{xx}[\omega_b] < \bar{S}^{(0)}_{xx}[\omega_b]$, as is the case of Fig. 3(a). Otherwise, for the parameters used, at blue detuning, the phonon linewidth is significantly reduced, which implies a sharper symmetrized spectrum, as the one in Fig. 3(b). Otherwise, the effects of backaction noise in the dynamical backaction evasion scheme, shown in Figs. 3(c,d), are less evident than in the triple resonance configuration: they are relevant in a narrower frequency range, and consist mostly of a frequency shift of the phonon resonance.

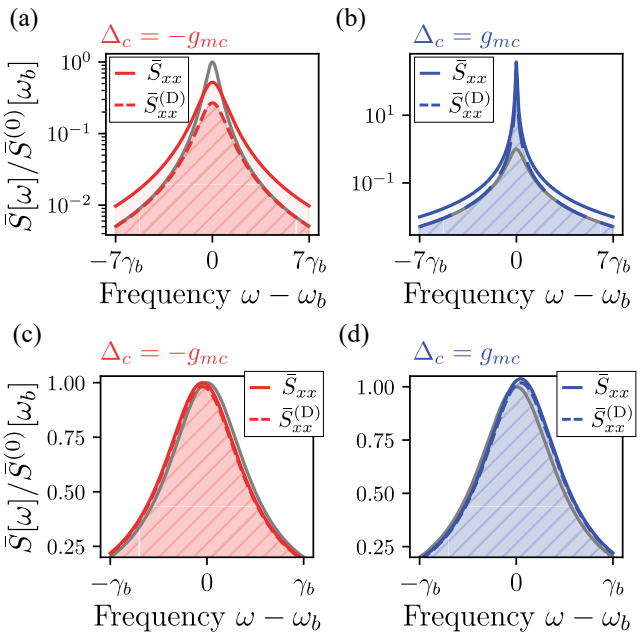

FIG. 3. Symmetrized noise spectrum around the phonon frequency for the triple resonance (a,b) and the dynamical backaction evasion (c,d) schemes and both red and blue detunings. The gray line depicts the noise spectrum for an uncoupled oscillator $\bar{S}^{(0)}_{xx}$, the dashed lines depict the contribution due to dynamical backaction $\bar{S}^{(\mathrm{D})}_{xx}$ (dashed lines), and the continuous line represents the total noise spectrum including the backaction noise $\bar{S}^{(\mathrm{BA})}_{xx}$ (see Eq. (23)). The shaded areas are a visual guide for the contributions of the different components of the noise spectrum. Plots for zero temperature and other parameters as in Table I.

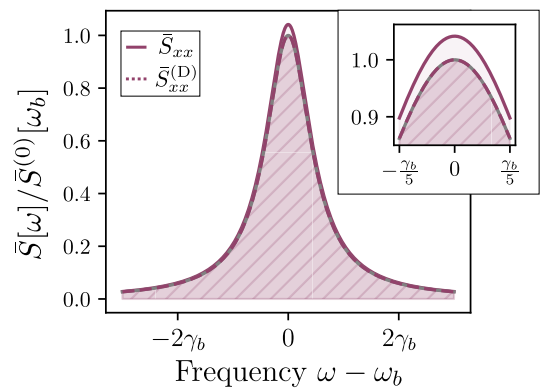

FIG. 4. (a) Symmetrized noise spectrum for $g_{mc} = \omega_b$ and $\Delta_c = 0$ (dynamical backaction evasion regime) for frequencies around the phonon frequency. The gray curve depicts the noise spectrum for an uncoupled oscillator, while the continuous magenta line corresponds to the total noise spectrum, including the backaction noise contribution $\bar{S}^{(\mathrm{BA})}_{xx}$ (see Eq. (23)). The shaded areas are a visual guide for the contributions of the different components of the noise spectrum. Plots for zero temperature and other parameters as in Table I.

At zero detuning, the magnomechanical self-energy vanishes irrespective of the scheme. In this case, $\bar{S}^{(D)}_{xx} = \bar{S}^{(0)}_{xx}$, (see equation 24), and any difference in the mechanics noise spectrum is due to quantum backaction. We show such a situation in Fig. 4 for the dynamical backaction evasion regime, and note that the difference between $\bar{S}_{xx}$ and the uncoupled value $\bar{S}^{(0)}_{xx}$ at zero detuning increases as the drive power or the magnomechanical coupling increase.

To quantify the amount of noise introduced at a given detuning, we now study the ratio between the integral of the total noise spectrum and its value for an uncoupled oscillator in thermal equilibrium. We show the comparison of I_{xx} with $I^{(0)}_{xx}$ in Fig. 5 for different phonon bath occupancies and for both the triple resonance and the dynamical backaction evasion scheme. The plots in Figs. 5(a,b) show sharp peaks at $\Delta_c = \pm g_{mc}$, which in both cases correspond to driving at the hybrid mode frequencies. At zero detuning Fig. 5c shows that $I_{xx} > I^{(0)}_{xx}$, which indicates, as anticipated by the results in Fig. 4, the presence of backaction noise even in a situation where dynamical backaction is evaded. At higher phonon temperatures $I_{xx} < I^{(0)}_{xx}$ depending on the detuning regime, which is associated with backaction cooling of the mechanics.

To end this section, we emphasize that the results presented here consider a rotating wave approximation (RWA) in which the last term in Eq. (9) is discarded. In the appendix, we present the full formulas, including such counter-rotating terms. All the results hold exactly for zero detuning since, in this case, the self-energy, which multiplies all counter-rotating terms, vanishes. The discarded counter-rotating terms can induce small corrections in I_{xx} [27], but as we show in the appendix, such corrections are still small enough to be safely discarded.

III. SCHEME FOR BACKACTION EVASION

The backaction noise can be eliminated from a quadrature of the phonon mode by considering a microwave drive containing two tones. In such a scheme the amplitude quadrature $\hat{x}(t) = (e^{-i\omega_b t}\hat{b} + e^{i\omega_b t}\hat{b})/\sqrt{2}$ of the phonon field will be a BAE quadrature, completely free of noise due to the coupling to magnons at all times. The drive term to be included in the magnomechanical Hamiltonian is

$$\frac{\hat{H}_{\mathrm{drive}}}{\hbar} = i\sqrt{\kappa_e}(\epsilon_- e^{-i\delta t} + \epsilon_+ e^{i\delta t})e^{i\omega_d t}\hat{c} + \mathrm{H.c.} \qquad (28)$$

This term describes two coherent tones applied to the microwave mode with frequencies $\omega_d \pm \delta$. To linearize the corresponding equations of motion, we again move to a rotating frame at the central drive frequency ω_d and

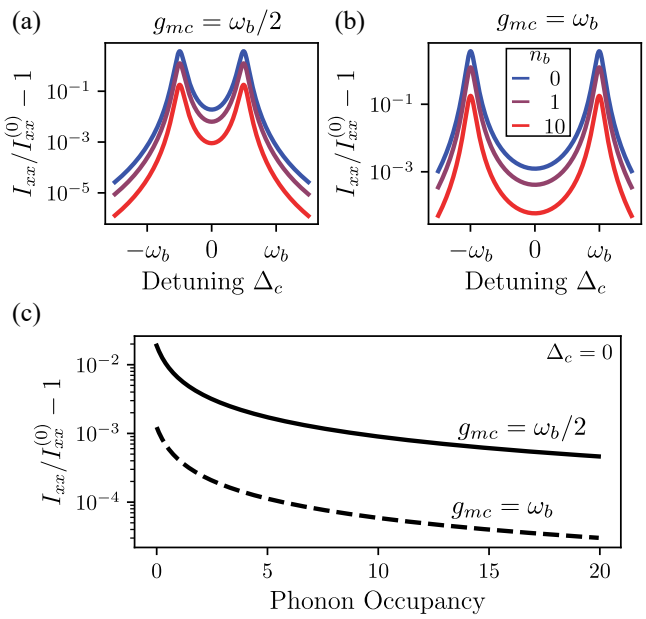

FIG. 5. Ratio the integral of noise spectrum and its value for an uncoupled oscillator at thermal equilibrium for (a) $g_{mc} = \omega_b/2$ (triple resonance scheme), and (b) $g_{mc} = \omega_b$ (dynamical backaction evasion scheme), as a function of the microwave-drive detuning Δ_c. (c) The ratio between the effective temperature defined by the integral of the noise spectrum and its value for an uncoupled oscillator at zero detuning as a function of the phonon occupancy n_b. Parameters as in Table I.

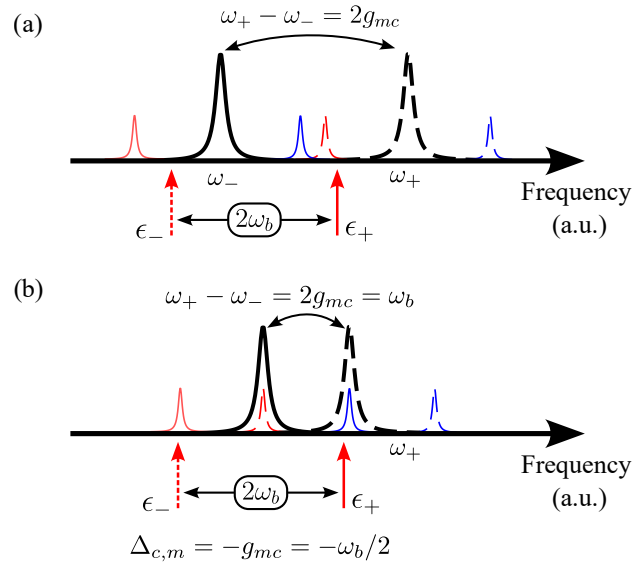

FIG. 6. Frequency configuration for the double drive backaction evasion scheme. (a) General framework: the two tones have to be separated by twice the phonon frequency and the drive amplitudes $\epsilon_\pm$ have to satisfy Eq. (34). The hybrid mode splitting can be arbitrary; (b) one particular configuration in which the mode splitting is set to the triple resonance scheme. In this case, the tones are centered around the lower hybrid mode. The high frequency tone drives simultaneously the blue sideband of the lower hybrid mode and the upper hybrid mode. As we will show in Section IV, such a configuration yields the minimum imprecision noise in the measurement of the BAE quadrature via the microwave output.

make the ansatz $\hat{c} = \hat{c}_0 + \hat{c}_+ e^{-i\delta t} + \hat{c}_- e^{i\delta t}$ and $\hat{m} = \hat{m}_0 + \hat{m}_+ e^{-i\delta t} + \hat{m}_- e^{i\delta t}$. We show the full set of equations for the expectation values $\langle \hat{o}_i \rangle = o_i$ ($o = m$, c, and $i = 0, \pm$) in the appendix. The steady-state solutions $\bar{o}_i$ are

$$\begin{aligned} \bar{c}_0 &= \bar{m}_0 = 0, \\ \bar{c}_\pm &= \frac{\sqrt{\kappa_e}\epsilon_\pm \left(i(\Delta_m \pm \delta) - \frac{\kappa_m}{2}\right)}{\left(i(\Delta_m \pm \delta) - \frac{\kappa_m}{2}\right)\left(i(\Delta_c \pm \delta) - \frac{\kappa_c}{2}\right) + g_{mc}^2}, \\ \bar{m}_\pm &= \frac{i g_{mc}\sqrt{\kappa_e}\epsilon_\pm}{\left(i(\Delta_m \pm \delta) - \frac{\kappa_m}{2}\right)\left(i(\Delta_c \pm \delta) - \frac{\kappa_c}{2}\right) + g_{mc}^2}. \end{aligned} \tag{29}$$

We have assumed that the single-magnon magnomechanical coupling is small, so we can ignore it in obtaining the mean-field steady-state solutions. The detunings with respect to the central drive frequency are given by $\Delta_{c,m} = \omega_d - \omega_{c,m}$, which we call from now on just detunings.

We linearize the two-tone drive Hamiltonian by considering fluctuations around the steady-state given by Eqs. (29): $\hat{\alpha} = \delta\hat{\alpha} + \bar{\alpha}_+ e^{-i\delta t} + \bar{\alpha}_- e^{i\delta t}$ for $\alpha = c, m$. We drop the deltas indicating the fluctuations and keep only the quadratic terms of the Hamiltonian. In an interacting frame with respect to $\omega_b \hat{b}^\dagger \hat{b}$, the Hamiltonian reads

$$\begin{aligned} \frac{\hat{H}_L^{(2)}}{\hbar} &= -\Delta_c \hat{c}^\dagger \hat{c} - \Delta_m \hat{m}^\dagger \hat{m} + g_{mc}\left(\hat{m}^\dagger \hat{c} + \hat{m}\hat{c}^\dagger\right) \\ &\quad + e^{i\delta t}\left(g_- \hat{m}^\dagger + g_+^* \hat{m}\right)\left(\hat{b}e^{-i\Omega_b t} + \hat{b}^\dagger e^{i\Omega_b t}\right) \\ &\quad + e^{-i\delta t}\left(g_+ \hat{m}^\dagger + g_-^* \hat{m}\right)\left(\hat{b}e^{-i\Omega_b t} + \hat{b}^\dagger e^{i\Omega_b t}\right), \end{aligned} \tag{30}$$

where we have defined $g_\pm = g_{mb}^0 \bar{m}_\pm$.

Since δ is positive, the interacting terms are resonant provided that $\delta = \omega_b$, in other words, if the two tones are separated by twice the phonon frequency as we schematically shown in Fig. 6. With this choice, a QND Hamiltonian for a phonon quadrature can be obtained by an appropriate choice of the magnomechanical coupling rates $g_\pm = |g_\pm| e^{i\phi_\pm}$. If coupling rates have the same modulus,

$$|g_-| = |g_+| = G, \tag{31}$$

we get after some algebraic manipulations

$$\begin{aligned} \frac{\hat{H}_{\rm QND}}{\hbar} &= -\Delta_c \hat{c}^\dagger \hat{c} - \Delta_m \hat{m}^\dagger \hat{m} + g_{mc}\left(\hat{m}^\dagger \hat{c} + \hat{m}\hat{c}^\dagger\right) \\ &\quad + G\left(e^{i\varphi}\hat{m}^\dagger + e^{-i\varphi}\hat{m}\right)\left(e^{i\psi}\hat{b}^\dagger + e^{-i\psi}\hat{b}\right), \end{aligned} \tag{32}$$

where $\varphi = (\phi_+ + \phi_-)/2$ and $\psi = (\phi_+ - \phi_-)/2$. The above Hamiltonian is QND with respect to the phonon quadrature

$$\hat{x}_{b,\psi} = \frac{e^{i\psi}\hat{b}^\dagger + e^{-i\psi}\hat{b}}{\sqrt{2}}, \tag{33}$$

meaning that the above quadrature is completely unaffected by the coupling to the magnons and by any measurement process done in the magnon-microwave part of the system. This quadrature is thus a BAE quadrature.

The requirement set in Eq. (31) corresponds to $|\bar{m}_+| = |\bar{m}_-|$; in other words, the drives induce the same amount of coherent magnons. Such a requirement implies the following relation between the drive amplitudes

$$\frac{|\epsilon_+|}{|\epsilon_-|} = \frac{|\left(i(\Delta_m+\omega_b) - \frac{\kappa_m}{2}\right)\left(i(\Delta_c+\omega_b) - \frac{\kappa_c}{2}\right) + g_{mc}^2|}{|\left(i(\Delta_m-\omega_b) - \frac{\kappa_m}{2}\right)\left(i(\Delta_c-\omega_b) - \frac{\kappa_c}{2}\right) + g_{mc}^2|}. \tag{34}$$

We note that only at zero detuning $\Delta_m = \Delta_c = 0$, the above equation implies an equal amplitude of both drives $|\epsilon_-| = |\epsilon_+|$. The phase ψ is given by the relative phase of the magnon steady-state solutions

$$\psi = \frac{\arg[\bar{m}_+] - \arg[\bar{m}_-]}{2}, \tag{35}$$

which can be tuned by, for example, a relative phase between the drive amplitudes $\epsilon_\pm$.

Unlike dynamical backaction evasion, the quantum nondemolition Hamiltonian does not require the detunings to vanish. Nevertheless, to obtain Eq. (32) we have adopted a RWA for discarding terms rotating at twice the phonon frequency. In this case, even at zero detuning, this RWA is not exact, and we discuss and evaluate the effects of the counter-rotating terms at zero detuning in the appendix. We show that, for the parameters considered here, the corrections that the counter-rotating terms introduce in the integral of the mechanics noise spectrum is $\sim 10^{-4}$, and therefore constitute a small correction that can be safely ignored. At finite detunings, the analysis is more involved, but we expect that the same conclusion still holds.

A. BAE phonon noise spectrum: orthogonal quadrature

In the last section, we have shown that a careful tuning of the two tones frequencies and amplitudes yields a QND Hamiltonian for the phonon quadrature (33). In turn, the conjugated quadrature

$$\hat{p}_{b,\psi} = \frac{i\left(e^{i\psi}\hat{b}^\dagger - e^{-i\psi}\hat{b}\right)}{\sqrt{2}}, \tag{36}$$

will be driven by the magnon-microwave noise. To quantify how much noise is dumped into $\hat{p}_{b,\psi}$, we calculate its noise spectrum. We start with the Heisenberg-Langevin equations for the phonon operator in the frequency domain, which reads

$$\begin{aligned}\left(\chi_b^{-1}[\omega] - i\Sigma_b[\omega]\right)e^{-i\psi}\hat{b}[\omega] &= ie^{i\psi}\Sigma_b[\omega]\hat{b}^\dagger[\omega] \\ -iGe^{i\varphi}\hat{\xi}_{\rm BA}^\dagger[\omega] - iGe^{-i\varphi}\hat{\xi}_{\rm BA}[\omega] &+ \sqrt{\gamma_b}\hat{\xi}_b[\omega],\end{aligned} \tag{37}$$

where, because now we are in an interacting frame of the phonon mode, the susceptibility χ_b is given by

$$\chi_b[\omega] = \frac{1}{-i\omega + \frac{\gamma_b}{2}}. \tag{38}$$

The phonon self-energy Σ_b is given by Eq. (11) with the substitution $g_{mb} \to G$, and the backaction noise operator $\hat{\xi}_{\rm BA}$ is given by Eq. (16). We then get the following equations for the BAE quadrature and its canonical conjugated quadrature

$$\begin{aligned}\chi_b^{-1}[\omega]\hat{x}_{b,\psi}[\omega] &= \sqrt{\gamma_b}\hat{\xi}_{x_{b,\psi}}[\omega], \\ \chi_b^{-1}[\omega]\hat{p}_{b,\psi}[\omega] &= \sqrt{\gamma_b}\hat{\xi}_{p_{b,\psi}}[\omega] - 2G\hat{\xi}_{{\rm BA},x_\varphi}[\omega] \\ &\quad + 2\Sigma_b[\omega]\chi_b[\omega]\hat{\xi}_{x_{b,\psi}}[\omega].\end{aligned} \tag{39}$$

The noise quadratures are defined as the other quadratures. As expected from the Hamiltonian in Eq. (32), the equation for $\hat{x}_{b,\psi}$ has no magnon-microwave noise. Otherwise, the non-BAE quadrature $\hat{p}_{b,\psi}[\omega]$ has two contributions in addition to thermal noise: the backaction noise $G\hat{\xi}_{{\rm BA},x_\varphi}[\omega]$ and the "dynamical backaction" noise $\Sigma_b[\omega]\chi_b[\omega]\hat{\xi}_{x_{b,\psi}}[\omega]$. In the case where both tones are perfectly centered around the magnon/microwave frequency, the last term vanishes.

The BAE quadrature noise spectrum is just the spectrum of an uncoupled oscillator at thermal equilibrium

$$\begin{aligned}S_{xx}[\omega] &= \int \frac{d\omega'}{2\pi}\langle\hat{x}_{b,\psi}[\omega]\hat{x}_{b,\psi}[\omega']\rangle \\ &= S^{(0)}[\omega] = \frac{\gamma_b(n_b+\frac{1}{2})}{\omega^2 + \frac{\gamma_b^2}{4}},\end{aligned} \tag{40}$$

while, at zero detuning ($\Delta_m = \Delta_c = 0$) the non-BAE quadrature noise spectrum is

$$\begin{aligned}S_{pp}[\omega] &= \int \frac{d\omega'}{2\pi}\langle\hat{p}_{b,\psi}[\omega]\hat{p}_{b,\psi}[\omega']\rangle \\ &= S^{(0)}[\omega] + S_{pp}^{({\rm BA})}[\omega].\end{aligned} \tag{41}$$

On top of the thermal noise $S^{(0)}[\omega]$ the quadrature is subjected to backaction noise $S_{pp}^{({\rm BA})}[\omega]$ given by

$$\begin{aligned}S_{pp}^{({\rm BA})}[\omega] = 4\frac{G^2|\Xi_m[\omega]|^2}{\omega^2 + \frac{\gamma_b^2}{4}}\Big[\kappa_m\left(n_m + \frac{1}{2}\right) \\ + g_{mc}^2\kappa_c|\chi_c[\omega]|^2\left(n_c + \frac{1}{2}\right)\Big].\end{aligned} \tag{42}$$

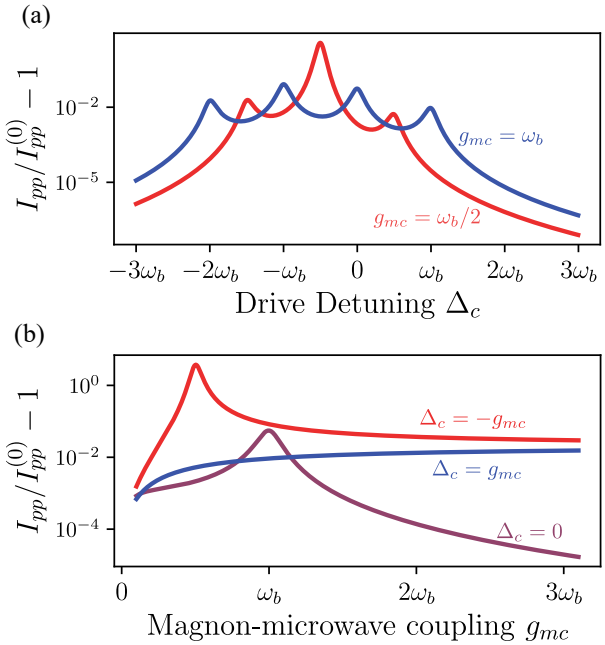

FIG. 7. Ratio between the uncertainty in the non-BAE quadrature $\hat{p}_\psi$ and the reference value for an uncoupled oscillator in thermal equilibrium (a) as a function of the detuning between the central frequency of the two-tones and the microwave frequency for the triple resonant scheme and the dynamical backaction evasion scheme, and (b) as a function of the magnon-microwave coupling for different values of Δ_c. Plots for zero temperature and all parameters as in Table I.

For $\Delta_m \neq \Delta_c \neq 0$, the non-BAE noise spectrum has further contributions due to the self-energy term, the last term in Eq. (39). We show the full formula for $S_{pp}[\omega]$ in the appendix. To compute the effects of backaction noise in the non-BAE quadrature of the phonon mode, we compute the integral of the noise spectrum

$$I_{pp} = \int \frac{d\omega}{2\pi} S_{pp}[\omega]. \tag{43}$$

We take the value for an uncoupled oscillator of the same frequency at thermal equilibrium value as a reference

$$I_{pp}^{(0)} = \int \frac{d\omega}{2\pi} S^{(0)}[\omega] = n_b + \frac{1}{2}. \tag{44}$$

In Fig. 7, we show the ratio I_{pp}/I_{pp}^0 as a function of the detuning Δ_c, and as a function of the magnon-microwave coupling. Different magnomechanics schemes yield different peaks in the added noise for the non-BAE quadrature. For the triple resonance scheme, we notice maxima of I_{pp} for detunings $\Delta_c = (-3\omega_b/2, -\omega_b/2, \omega_b/2)$, while for the dynamical backaction evasion scheme the maxima are at $\Delta_c = (-2\omega_b, -\omega_b, 0, \omega_b)$. We can understand the position of these peaks by considering the hybrid mode formation in each case. For example, in the case of the highest peak shown in Fig. 7(a), since $g_{mc} = \omega_b/2$, the magnon-microwave hybrid modes are located at $\omega_c \pm \omega_b/2$. The red sideband of the upper hybrid mode coincides with the frequency of the lower hybrid mode, and the blue sideband of the lower hybrid mode coincides with the frequency of the higher hybrid mode. When the detuning is set at $\Delta_c = -\omega_b/2$, the high-frequency drive is at the frequency of the upper hybrid mode, driving it and the blue sideband of the lower hybrid mode while the low-frequency drive is at the red sideband of the lower hybrid mode.

We should notice that the above analysis was performed considering a RWA. As we pointed out in the Appendix, the inclusion of discarded terms does break the BAE nature of the scheme, and, as a consequence, modifications of the noise spectrum of the quadrature $\hat{p}_\psi$ and its integral are expected.

B. Deviations from the quantum backaction evasion requirements

There are two requirements for BAE: the two tones applied to the microwave have to be separated by $2\delta = 2\omega_b$, and the amplitude of the tones has to be such that equation (34) is satisfied. Nevertheless, it might be hard to achieve such requirements perfectly in practical setups. We quantify how deviations from those requirements impact the effectiveness of BAE in the setup by studying I_{xx} when the quantum backaction evasion conditions are not met. We show all the formulas for the noise spectrum in the appendix and focus here on evaluating the results.

First, we consider an imperfect frequency difference δ, but assume that the drive amplitudes satisfy Eq. (34). The result for the integral I_{xx} as a function of δ is shown in Fig. 8 for both the triple resonance (a) and the backaction evasion (b) setups, and at zero temperature. The triple resonance case at zero detuning exhibits the smallest difference from the uncoupled value, while the same scheme at $\Delta_c = g_{mc}$ (tones centered around the upper hybrid mode) adds more noise to the quadrature. The deviations from the BAE condition become relevant for $|\delta - \omega_b| > \gamma_b/2$, and thus, mechanical modes with larger dissipation rates should be more robust for the BAE scheme. We emphasize that at zero detuning $\Delta_c = 0$, i.e., there is no dynamical backaction and any modification of the phonon noise is due entirely to quantum backaction.

In Fig. 9, we show the case where the drive amplitudes do not satisfy the relation set in Eq. (34), but the frequency difference between the tones is $2\delta = 2\omega_b$. In this case, we consider deviations of the lower frequency drive amplitude $|\epsilon_-|$ from the BAE value $|\epsilon_0|$ given by Eq. (34). Similar to the previous case, deviations from the backaction evasion regime are more prominent for the triple resonance scheme and tones centered around the lower hybrid mode frequency. Furthermore, we notice that the deviations from the uncoupled position

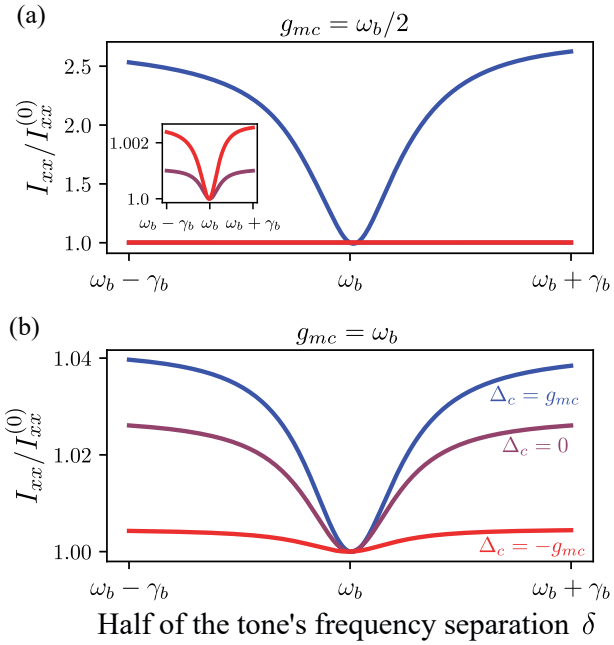

FIG. 8. Integral of the position noise spectrum $I_{xx} = \langle \hat{x}^2_{b,\psi} \rangle$ as a function of half of the tone's frequency separation δ for (a) the triple resonance scheme $g_{mc} = \omega_b/2$ and (b) for the dynamical backaction evasion scheme $g_{mc} = \omega_b$. Plots for zero temperature and all parameters as in Table I.

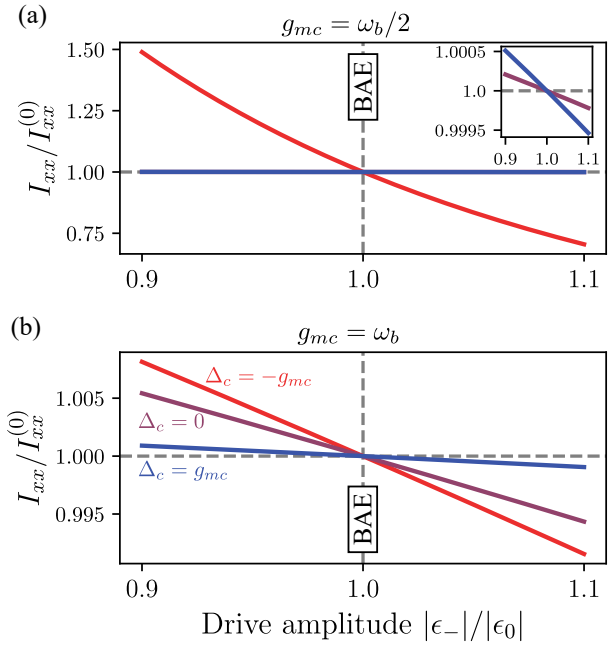

FIG. 9. Integral of the position noise spectrum $I_{xx} = \langle \hat{x}^2_{b,\psi} \rangle$ as a function of the lower frequency drive amplitude $|\epsilon_-|$ for (a) the triple resonance scheme $g_{mc} = \omega_b/2$ and (b) the dynamical backaction evasion scheme $g_{mc} = \omega_b$. In these plots the tones frequency difference is set at $2\delta = 2\omega_b$. Plots for zero temperature and all parameters as in Table I.

uncertainty $I_{xx}^{(0)}$ are approximately linear with the drive amplitude. Another prominent feature is that for $|\epsilon_-| > |\epsilon_0|$, the quadrature fluctuations I_{xx} go below the value of the zero-point fluctuations, indicating squeezing of the quadrature. Mechanical squeezing induced by a two-tone *magnon drive* was theoretically studied in [30] and the induced microwave squeezing in a two-tone drive setup was recently investigated in [31].

IV. MICROWAVE OUTPUT SPECTRUM

We now turn our attention to the measurement of the BAE quadrature via the output microwave signal. For this, we consider the standard input-output relation

$$\hat{c}_{\rm out}[\omega] = \hat{\xi}_c[\omega] - \sqrt{\kappa_c}\hat{c}[\omega], \tag{45}$$

where we have assumed that the only source of input noise is thermal. We then consider the noise spectrum of the output quadrature

$$\hat{x}_{{\rm out},\theta}[\omega] = \frac{e^{i\theta}\hat{c}^\dagger_{\rm out}[\omega] + e^{-i\theta}\hat{c}_{\rm out}[\omega]}{\sqrt{2}}, \tag{46}$$

given by

$$S_{\theta\theta}[\omega] = \int \frac{d\omega'}{2\pi} \langle \hat{x}_{{\rm out},\theta}[\omega]\hat{x}_{{\rm out},\theta}[\omega'] \rangle. \tag{47}$$

The symmetrized version of (47) consists of dips associated with the hybrid modes response. On top of such spectrum, there will be a Lorentzian centered around $\omega = 0$, which is the signal of the BAE quadrature. In fact, for frequencies in an interval close to zero, we can write

$$S_{\theta\theta}[\omega] = |\mathcal{G}_{x,\theta}[\omega]|^2 \left[S^{(0)}[\omega] + \frac{4n_{{\rm imp},\theta}}{\gamma_b} \right], \tag{48}$$

where $n_{{\rm imp},\theta}$ is an effective number of quanta added to the measurement of the mechanical spectrum due to the imprecision noise. Since the scheme is BAE, there is no noise added by backaction. The explicit expression for the coefficient $\mathcal{G}_{x,\theta}[\omega]$, representing the measurement gain, and the added number of quanta $n_{{\rm imp},\theta}$ is given in the appendix.

The added quanta $n_{{\rm imp},\theta}$ depends non-trivially on the quadrature angle θ and can be minimized by a judiciously chosen measured output quadrature. The measurement scheme that yields a small amount of added imprecision noise can be obtained by optimizing the output quadrature angle. We indicate the angle that minimizes $n_{{\rm imp},\theta}$ for a given drive detuning and magnon-microwave coupling as $\theta_{\rm opt}$. In Fig. 10, we show the result for the corresponding optimal added quanta as a function of the drive-detuning $\Delta_c = \Delta_m$ for magnon-microwave couplings ranging from $\omega_b/2$ (triple resonance) to ω_b (dynamical backaction evasion). The minimum

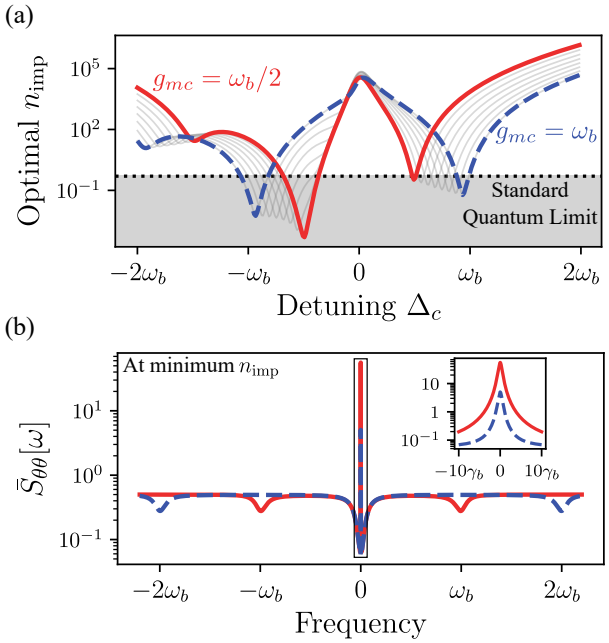

FIG. 10. (a) Number of added quanta due to imprecision noise for the optimal output quadrature as a function of the cavity-drive detuning Δ_c for magnon-microwave couplings ranging from $\omega_b/2$ (red curve) to ω_b (blue-dashed curve). The gray curves correspond to intermediate values of g_{mc}. The dotted line indicates the standard quantum limit for added noise $n_{\rm imp}^{\rm SQL} = 1/2$. (b) Symmetrized microwave output spectrum at the minimum of the added noise for $g_{mc} = \omega_b/2$ and $g_{mc} = \omega_b$. The inset shows the noise spectrum in a narrow frequency range around 0 corresponding to the BAE quadrature. Plots for zero temperature and all parameters as in Table I.

added imprecision noise to the BAE measurement is obtained in the triple resonance scheme for a detuning set at the lower hybrid mode. In this case, the high-frequency tone is at the higher hybrid mode, while the lower-frequency tone is at the red mechanical sideband of the lower hybrid mode. The optimal quadrature angle is $\theta_{\rm opt} \approx -0.43\pi$, which yields, for the parameters used here, a minimum of added quanta of $\sim 10^{-3}$. This point corresponds to the maximum signal-to-noise ratio, as we can infer from Fig. 10(b), where we show the symmetrized microwave output noise spectrum for the optimal quadrature in both the triple resonance and the dynamical backaction evasion schemes. The mechanical signal peak is more pronounced when compared to the background imprecision noise for the first case.

Under the assumption that the counter-rotating terms appearing in the solutions for $\hat{x}_{\psi,b}[\omega]$ can be discarded and for perfect detection efficiency, the imprecision noise $n_{\rm imp}$ can be made arbitrarily small by increasing the driving amplitude, which is limited by the system stability conditions. In such a perfect scenario, the added quanta to the measurement can go below the standard quantum limit (SQL), $n_{\rm imp}^{\rm SQL} = 1/2$, for drives centered around the hybrid modes. The imprecision added noise, in this case, is mainly determined by the thermal occupation of the magnon and microwave baths and by the drives amplitudes, as such, $n_{\rm imp}$ can be below the SQL even at moderately high temperatures. The RWA performed should hold in the 'good cavity' regime $\kappa_{c,m} < \omega_b$ and for weak magnomechanical couplings but, analogously to standard optomechanical system [3], we expect that such a scheme can cope with small deviations from the perfect BAE measurement and still be able to beat the standard quantum limit.

Finally, the added imprecision quanta depends on the magnon/microwave bath occupancy and on the drive power (see the Appendix). For the parameters we considered here, the scheme is able to beat the SQL for magnon/microwave bath occupancies up to a few hundred quanta, while at weaker drive powers the bath temperature has to be smaller. We notice, however, that for magnon/microwave modes with $\sim$ 10 GHz frequencies, a negligible occupancy can be attained at a few hundreds of mK, which is routinely achieved in cavity magnonic experiments [35, 42].

V. CONCLUSION

To summarize, we have characterized the quantum noise added to mechanical vibrations in cavity magnomechanical systems and proposed a two-tone drive scheme to implement a backaction evasion measurement of a mechanical quadrature. Different schemes for backaction evasion are possible, and we have studied their robustness to imperfections of the BAE requirements, as well as the amount of noise added in relevant schemes on the measurement via the output of the microwave mode. The effectiveness of BAE in our proposal is more robust to imperfections for a vanishing microwave detuning (both tones centered at the microwave frequency). Nevertheless, this case corresponds to the maximum imprecision noise added to the measurement of the BAE phonon quadrature. Otherwise, by centering the tones around the hybrid magnon-microwave modes, even though the scheme is less robust to imperfections, less imprecision noise is added to the measurement. In fact, in this case, it is possible to go below the standard quantum limit.

Our results provide a potential route for measuring phonons in cavity magnomechanical systems. For instance, such a quantum backaction evasion scheme can be used to perform quantum tomography of phonons and validate the creation of entangled states proposed in the literature. A more complete model should include imperfect measurement efficiency as well as other intrinsic features of cavity magnomechanical systems, in particular magnetic nonlinearities and the unavoidable coupling to high order Walker modes [33]. As we have shown previously, both nonlinearities and the coupling to several magnon modes change dynamical backaction, and the same should be true for the quantum backaction

studied here. Still, a double-drive BAE scheme should be possible, with small modifications due to the change in the magnon and phonon frequencies stemming from nonlinearities and the coupling to multiple magnon modes, an analysis that we postpone to future work.

Acknowledgements V.A.S.V.B. and A.M. acknowledge financial support from the Contrat Triennal 2021-2023 Strasbourg Capitale Europeenne. C.A.P. acknowledges the support of the Natural Sciences and Engineering Research Council, Canada (NSERC). J.P.D. acknowledges funding support from the NSERC (Grant Nos. RGPIN-2022-03078, and CREATE-495446-17); Alberta Innovates; and the Government of Canada through the NRC Quantum Sensors Program.

APPENDIX

A. Backaction noise correlators

In the main text, we have defined the backaction noise $\hat{\xi}_{\rm BA}$ in eq. (16):

$$\hat{\xi}_{\rm BA}[\omega] = \Xi_m[\omega](\sqrt{\kappa_m}\hat{\xi}_m[\omega] - ig_{mc}\sqrt{\kappa_c}\chi_c[\omega]\hat{\xi}_c[\omega]). \tag{1}$$

Throughout the paper, we consider that the magnon and microwave noises $\hat{\xi}_{c,m}[\omega]$ are thermal, with correlations given in eqs. (8). We have then the following correlations for $\hat{\xi}_{\rm BA}$:

$$\begin{aligned}
\langle\hat{\xi}_{\rm BA}[\omega]\hat{\xi}_{\rm BA}[\omega']\rangle &= \langle\hat{\xi}^\dagger_{\rm BA}[\omega]\hat{\xi}^\dagger_{\rm BA}[\omega']\rangle = 0\\
\langle\hat{\xi}_{\rm BA}[\omega]\hat{\xi}^\dagger_{\rm BA}[\omega']\rangle &= 2\pi\Xi_m[\omega]\Xi^*_m[-\omega']\left(\kappa_m(n_m+1) + g^2_{mc}\kappa_c\chi_c[\omega]\chi^*_c[-\omega'](n_c+1)\right)\delta(\omega+\omega')\\
\langle\hat{\xi}^\dagger_{\rm BA}[\omega]\hat{\xi}_{\rm BA}[\omega']\rangle &= 2\pi\Xi^*_m[-\omega]\Xi_m[\omega']\left(\kappa_m n_m + g^2_{mc}\kappa_c\chi^*_c[-\omega]\chi_c[\omega']n_c\right)\delta(\omega+\omega')
\end{aligned} \tag{2}$$

B. Effects of the counter-rotating term on the mechanics noise spectrum for a single tone drive

In section II, we have discarded a counter-rotating term in the solution for the phonon operator in frequency space. We now asses the impact of this discarded term in the results presented in the main text.

The solution for the phonon operator obtained from the linearized Heisenberg-Langevin equation in frequency space, Eq. (9), reads

$$\tilde{\chi}_b^{-1}[\omega]\hat{b}[\omega] = -i\hat{f}_{\rm BA}[\omega] + \sqrt{\gamma_b}\hat{\xi}_b[\omega] + i\Sigma_b[\omega]\hat{b}^\dagger[\omega]. \tag{3}$$

The counter-rotating term induces squeezing which depends on the "bare" self-energy $\Sigma_b[\omega]$. For the dynamical backaction evasion scheme, i.e., for $g_{mc} = \omega_b$ and $\Delta_c = 0$, such counter-rotating term has no effect since in such parameter regime $\Sigma_b[\omega] = 0$. In any case, the full solution for the phonon operator in frequency domain is given by

$$\chi^{-1}_{b,\rm eff}[\omega]\hat{b}[\omega] = -iF_{\rm BA}[\omega]\hat{f}_{\rm BA}[\omega] + \sqrt{\gamma_b}\hat{\xi}_b[\omega] + i\sqrt{\gamma_b}\Lambda[\omega]\hat{\xi}^\dagger_b[\omega]. \tag{4}$$

The effective phonon susceptibility including the counter-rotating term is

$$\chi^{-1}_{b,\rm eff}[\omega] = \chi^{-1}_b[\omega] - i\Sigma_b[\omega]\left(1 - \frac{i\Sigma_b[\omega]}{\chi^{-1,*}_b[\omega] + i\Sigma_b[\omega]}\right). \tag{5}$$

The pre-factor of the backaction noise term $\hat{f}_{\rm BA}$ is given by

$$\begin{aligned}
F_{\rm BA}[\omega] &= 1 - i\Lambda[\omega]\\
\Lambda[\omega] &= \frac{\Sigma_b[\omega]}{\chi^{-1,*}_b[\omega] + i\Sigma_b[\omega]}.
\end{aligned} \tag{6}$$

With those modifications of the phonon susceptibility and the pre-factors of the noise terms, the position noise spectrum reads

$$S_{xx}[\omega] = S^{(\rm D)}_{xx}[\omega] + S^{(\rm BA)}_{xx}[\omega], \tag{7}$$

where now the dynamical backaction term $S^{(\rm D)}_{xx}[\omega]$ reads

$$\begin{aligned}
S^{(\rm D)}_{xx}[\omega] &= \gamma_b\left[(n_b+1)|F_b[\omega]|^2 + n_b|F_b[-\omega]|^2\right]\\
F_b[\omega] &= \chi_{b,\rm eff}[\omega] - \chi^*_{b,\rm eff}[-\omega]\Lambda^*[-\omega].
\end{aligned} \tag{8}$$

Compared with the contribution without the counter-rotating term, given in Eq. (24), the effective susceptibility is substituted by the new effective susceptibility plus a term related to the squeezing induced by the counter-rotating term. The backaction noise contribution reads

$$\begin{aligned}
S^{(\rm BA)}_{xx}[\omega] = \kappa_c g^2_{mc}|g_{mb}\mathcal{F}_{\rm BA}[\omega]|^2|\chi_c[\omega]|^2\Big[|\Xi_m[-\omega]|^2 n_c + |\Xi_m[\omega]|^2(n_c+1)\Big]\\
+ \gamma_m|g_{mb}\mathcal{F}_{\rm BA}[\omega]|^2\Big[|\Xi_m[-\omega]|^2 n_m + |\Xi_m[\omega]|^2(n_m+1)\Big],
\end{aligned} \tag{9}$$

where now the function $\mathcal{F}_{\rm BA}[\omega]$ reads

$$\mathcal{F}_{\rm BA}[\omega] = F_{\rm BA}[\omega]\chi_{b,\rm eff}[\omega] - F^*_{\rm BA}[-\omega]\chi^*_{b,\rm eff}[-\omega]. \tag{10}$$

Similar to the dynamical backaction term, the difference is the modification of the effective phonon susceptibility plus a term related to squeezing.

All the corrections due to the counter-rotating term appearing in equation (9) have the phonon self-energy $\Sigma_b[\omega]$ as a pre-factor. For the case where magnons and microwaves are in resonance and a zero detuned drive $\Delta_c = 0$, the phonon self-energy vanishes and the full formulas shown here coincide with the simplifyied versions given in the main text. In the case where dynamical backaction is present, the counter-rotating terms induce small corrections in the quantities that we have studied in the main text.

In Fig. 1, we show the difference between the full symmetrized noise spectrum and the noise spectrum shown in the main text, for the triple resonance and the dynamical backaction evasion schemes and drive detunings $\Delta_c = \pm g_{mc}$, corresponding to the situations studied in the main text in Fig. 3. For a red detuned drive and both schemes, the maximum difference between the noise spectra is $\sim 10^{-6}$ the reference value $S^{(0)}_{xx}[\omega_b]$, 5 orders of magnitude smaller than the difference between the noise spectrum computed in the main text and the uncoupled position noise spectrum. Otherwise, the counter-rotating terms introduce a difference $\sim 10\%$ with respect to the reference value for a blue detuned drive in the triple resonance scheme, nevertheless, the difference itself is 4 order of magnitude smaller than the peaks. Moreover, such a difference is relevant in a frequency range narrower than the other cases.

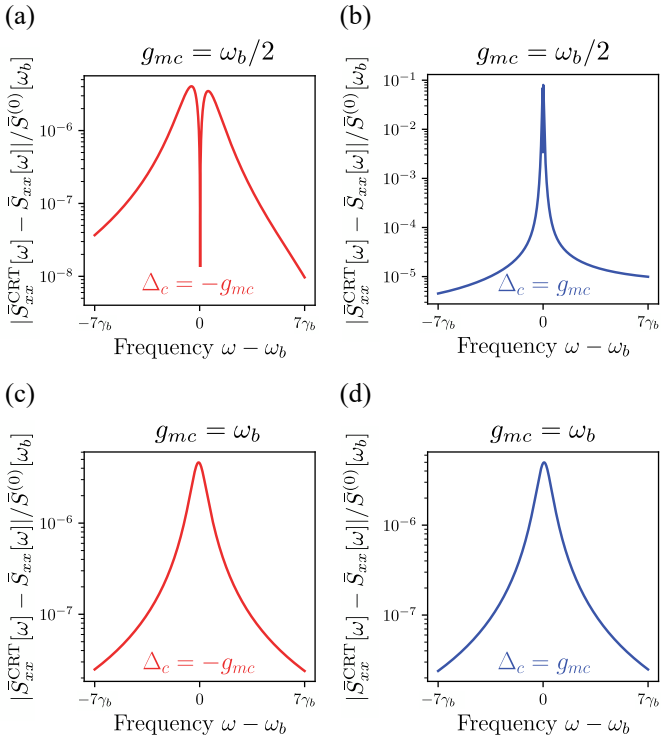

FIG. 1. Difference between the full noise spectrum and the noise spectrum not including the counter-rotating term discarded in Eq. (9) for frequencies around the phonon frequency. (a,b) for the triple resonance scheme, (c,d) for the dynamical backaction evasion scheme. Plots for zero temperature $n_b = n_c = n_m = 0$ and other parameters as in Table I.

We show the effects of the counter-rotating term in the integral of the mechanics noise spectrum I_{xx} in Fig. 2. The ratio between the integral of the full noise spectrum and the integral of the noise spectrum shown in the main text is shown as a function of the detuning, and we see that the largest difference is for detunings at the hybrid modes $\pm g_{mc}$. The maximum difference to the value with the RWA is $\sim 10^{-5}$. This difference is also two orders of magnitude smaller than the ratio of effective and uncoupled temperature at zero detuning. We also notice that the corrections are approximately independent from the phonon bath occupancy n_b.

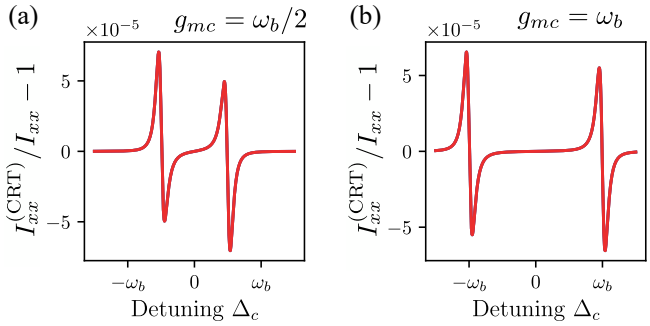

FIG. 2. Ratio between the integrals of the mechanics noise spectra with and without the discarded counter-rotating term for (a) the triple resonance scheme and (b) the dynamical backaction evasion scheme. Parameters as in Table I.

C. Heisenberg-Langevin equations for two-tones drive

The cavity magnomechanics Hamiltonian with the two-tones drive given in Eq. (28) reads:

$$\begin{aligned}\frac{\hat{H}}{\hbar} &= \omega_c \hat{c}^\dagger \hat{c} + \omega_m \hat{m}^\dagger \hat{m} + \omega_b \hat{b}^\dagger \hat{b} \\ &+ g_{mc}\left(\hat{m}^\dagger \hat{c} + \hat{m}\hat{c}^\dagger\right) + g_{mb}^0 \hat{m}^\dagger \hat{m}\left(\hat{b}^\dagger + \hat{b}\right) \\ &+ i\sqrt{\kappa_e}(\epsilon_- e^{-i\delta t} + \epsilon_+ e^{i\delta t})e^{i\omega_d t}\hat{c} + \mathrm{H.c.}.\end{aligned} \tag{11}$$

To obtain the semiclassical steady-state we move to an interacting frame rotating with $\omega_d \hat{c}^\dagger \hat{c} + \omega_d \hat{m}^\dagger \hat{m}$ and make the ansatz $\hat{c} = \hat{c}_0 + \hat{c}_+ e^{-i\delta t} + \hat{c}_- e^{i\delta t}$ and $\hat{m} = \hat{m}_0 + \hat{m}_+ e^{-i\delta t} + \hat{m}_- e^{i\delta t}$. Within a mean field approximation, the equations for the expectation values of each bosonic operator reads

$$\begin{aligned}\dot{c}_0 &= \left(i\Delta_c - \frac{\kappa}{2}\right)c_0 - i g_{mc} m_0, \\ \dot{c}_\pm &= \left(i(\Delta_c \pm \delta) - \frac{\kappa}{2}\right)c_\pm - i g_{mc} m_\pm - \sqrt{\kappa_e}\epsilon_\pm, \\ \dot{m}_0 &= \left(i\Delta_m - \frac{\gamma}{2}\right)m_0 - i g_{mc} c_0 - i g_{mb}^0 (m_- b + m_+ b^*), \\ \dot{m}_+ &= \left(i(\Delta_m + \delta) - \frac{\gamma}{2}\right)m_+ - i g_{mc} c_+ - i g_{mb}^0 m_0 b, \\ \dot{m}_- &= \left(i(\Delta_m - \delta) - \frac{\gamma}{2}\right)m_- - i g_{mc} c_- - i g_{mb}^0 m_0 b^*, \\ \dot{b} &= \left(i\Delta_b - \frac{\Gamma}{2}\right)b - i g_{mb}^0 (m_0^* m_+ + m_-^* m_0).\end{aligned} \tag{12}$$

We have discarded all terms $\propto e^{\pm 2i\delta t}$. The steady-state is obtained by setting all time derivatives to zero and solving the system of equations. In doing so, we assume the bare magnomechanical coupling g_{mc}^0 small enough to be ignored in the dynamics of the magnon and microwave amplitudes. Such a procedure gives Eqs. (29).

D. Solution for the phonon operator in the linearized two-tone driving scheme

We define $\delta_b = \omega_b - \delta$ and $\sigma_b = \omega_b + \delta$. In an interacting frame rotating with $\omega_b \hat{b}^\dagger \hat{b}$, we have the following equation for $\hat{m}[\omega]$ as a function of phonon operators

$$\hat{m}[\omega] = -i g_- \Xi[\omega]\left(\hat{b}[\omega - \delta_b] + \hat{b}^\dagger[\omega + \sigma_b]\right) - i g_+ \Xi[\omega](\hat{b}[\omega - \sigma_b] + \hat{b}^\dagger[\omega + \delta_b]) + \hat{\xi}_{\mathrm{BA}}[\omega], \tag{13}$$

where the modified magnon susceptibility $\Xi[\omega]$ and the backaction noise $\hat{\xi}_{\mathrm{BA}}[\omega]$ have the same formula as in the single drive case. The equation for the phonon operator reads

$$\chi_b^{-1}[\omega]\hat{b}[\omega] = -i g_- \hat{m}^\dagger[\omega + \sigma_b] - i g_+ \hat{m}^\dagger[\omega + \delta_b] - i g_-^* \hat{m}[\omega + \delta_b] - i g_+^* \hat{m}[\omega + \sigma_b] + \sqrt{\gamma_b}\hat{\xi}_b[\omega]. \tag{14}$$

Notice that in this frame $\chi_b[\omega] = (-i\omega + \gamma_b/2)^{-1}$.

Eliminating the magnon operator in favor of the phonon operators gives

$$\begin{aligned}\chi_b^{-1}[\omega]\hat{b}[\omega] &= i\Sigma_{b,\mathrm{T}}[\omega]\hat{b}[\omega] + i\Sigma_{b,\mathrm{T}}[\omega]\hat{b}^\dagger[\omega+2\omega_b] + f_1[\omega]\hat{b}[\omega+2\delta] + f_1[\omega]\hat{b}^\dagger[\omega+2\sigma_b] \\ &+ f_2[\omega]\hat{b}[\omega-2\delta] + f_2[\omega]\hat{b}^\dagger[\omega+2\delta_b] - ig_+\hat{\xi}^\dagger_{\mathrm{BA}}[\omega+\delta_b] - ig_-^*\hat{\xi}_{\mathrm{BA}}[\omega+\delta_b] \\ &- ig_-\hat{\xi}^\dagger_{\mathrm{BA}}[\omega+\sigma_b] - ig_+^*\hat{\xi}_{\mathrm{BA}}[\omega+\sigma_b] + \sqrt{\gamma_b}\hat{\xi}_b[\omega],\end{aligned} \tag{15}$$

In the above expression, the total phonon self-energy $\Sigma_{b,\mathrm{T}}[\omega]$ is given by

$$\Sigma_{b,\mathrm{T}}[\omega] = \Sigma_b[\omega] + \Sigma_{b,\mathrm{CRT}}[\omega], \tag{16}$$

where the co-rotating contribution $\Sigma_b[\omega]$ is given by

$$\Sigma_b[\omega] = i|g_-|^2\Xi_m[\omega+\delta_b] - i|g_+|^2\Xi_m^*[-\omega-\delta_b], \tag{17}$$

which is similar to that obtained for the one tone drive case, while the *counter-rotating* contribution is

$$\Sigma_{b,\mathrm{CRT}}[\omega] = i|g_+|^2\Xi_m[\omega+\sigma_b] - i|g_-|^2\Xi_m^*[-\omega-\sigma_b]. \tag{18}$$

The pre-factor functions $f_{1,2}[\omega]$ are given by

$$\begin{aligned}f_1[\omega] &= g_-g_+^*\left(\Xi_m^*[-\omega-\sigma_b] - \Xi_m[\omega+\sigma_b]\right), \\ f_2[\omega] &= g_-^*g_+\left(\Xi_m^*[-\omega-\delta_b] - \Xi_m[\omega+\delta_b]\right).\end{aligned} \tag{19}$$

1. *Mechanics noise spectrum in the BAE scheme*

The BAE scheme requires that $\delta_b = 0$ and $|g_+| = |g_-| = G$. Using the same notation of the main text $g_\pm = Ge^{i\pm\varphi_\pm}$, we obtain for the pre-factors

$$\begin{aligned}\Sigma_{b,\mathrm{T}}[\omega] &= \Sigma_b[\omega] + \Sigma_{b,\mathrm{CRT}}[\omega], \\ \Sigma_b[\omega] &= iG^2\left(\Xi_m[\omega] - \Xi_m^*[-\omega]\right), \\ \Sigma_{b,\mathrm{CRT}}[\omega] &= iG^2\left(\Xi_m[\omega+2\omega_b] - \Xi_m^*[-\omega-2\omega_b]\right), \\ f_1[\omega] &= -G^2e^{-i(\varphi_+-\varphi_-)}\left(\Xi_m[\omega+2\omega_b] - \Xi_m^*[-\omega-2\omega_b]\right) = ie^{-i(\varphi_+-\varphi_-)}\Sigma_{b,\mathrm{CRT}}[\omega] \\ f_2[\omega] &= -G^2e^{i(\varphi_+-\varphi_-)}\left(\Xi_m[\omega] - \Xi_m^*[-\omega]\right) = ie^{i(\varphi_+-\varphi_-)}\Sigma_b[\omega].\end{aligned} \tag{20}$$

and the phonon operator is given by

$$\begin{aligned}\chi_b^{-1}[\omega]\hat{b}[\omega] &= i\Sigma_b[\omega]\hat{b}[\omega] + i\Sigma_{b,\mathrm{CRT}}[\omega]\hat{b}[\omega] + i\Sigma_{b,\mathrm{T}}[\omega]\hat{b}^\dagger[\omega+2\omega_b] \\ &+ ie^{-2i\psi}\Sigma_{b,\mathrm{CRT}}[\omega]\left(\hat{b}[\omega+2\omega_b] + \hat{b}^\dagger[\omega+4\omega_b]\right) \\ &+ ie^{2i\psi}\Sigma_b[\omega]\left(\hat{b}^\dagger[\omega] + \hat{b}[\omega-2\omega_b]\right) \\ &- iGe^{i(\psi+\varphi)}\hat{\xi}^\dagger_{\mathrm{BA}}[\omega] - iGe^{i(\psi-\varphi)}\hat{\xi}_{\mathrm{BA}}[\omega] \\ &- iGe^{-i(\psi-\varphi)}\hat{\xi}^\dagger_{\mathrm{BA}}[\omega+2\omega_b] - iGe^{-i(\psi+\varphi)}\hat{\xi}_{\mathrm{BA}}[\omega+2\omega_b] + \sqrt{\gamma_b}\hat{\xi}_b[\omega],\end{aligned} \tag{21}$$

where we have explicitly separated rotating and counter-rotating contributions for the self-energy in the first term and we have used the definitions. We have defined the phases ψ and ϕ as

$$\begin{aligned}\psi &= \frac{\varphi_+ - \varphi_-}{2}, \\ \varphi &= \frac{\varphi_+ + \varphi_-}{2}.\end{aligned} \tag{22}$$

After some algebraic manipulations, from eq. (21) we obtain the following equation for the quadrature $\hat{x}_{b,\psi}$ defined in eq. (33)

$$\begin{aligned}\sqrt{2}\chi_b^{-1}[\omega]\hat{x}_{b,\psi}[\omega] = &\sqrt{2\gamma_b}\hat{\xi}_{x_{b,\psi}}[\omega] \\ &+ i\Sigma_{b,\mathrm{CRT}}[\omega]e^{-i\psi}\hat{b}[\omega] - i\Sigma^*_{b,\mathrm{CRT}}[-\omega]e^{i\psi}\hat{b}^\dagger[\omega] \\ &+ ie^{-3i\psi}\Sigma_{b,\mathrm{CRT}}[\omega]\left(\hat{b}[\omega+2\omega_b] + \hat{b}^\dagger[\omega+4\omega_b]\right) - ie^{3i\psi}\Sigma^*_{b,\mathrm{CRT}}[-\omega]\left(\hat{b}^\dagger[\omega-2\omega_b] + \hat{b}[\omega-4\omega_b]\right) \\ &+ i\Sigma_b[\omega]\left(e^{i\psi}\hat{b}[\omega-2\omega_b] - e^{-i\psi}\hat{b}^\dagger[\omega+2\omega_b]\right) \\ &- iGe^{-i(2\psi-\varphi)}\hat{\xi}^\dagger_{\mathrm{BA}}[\omega+2\omega_b] + iGe^{i(2\psi-\varphi)}\hat{\xi}_{\mathrm{BA}}[\omega-2\omega_b] \\ &- iGe^{-i(2\psi+\varphi)}\hat{\xi}_{\mathrm{BA}}[\omega+2\omega_b] + iGe^{i(2\psi+\varphi)}\hat{\xi}^\dagger_{\mathrm{BA}}[\omega-2\omega_b].\end{aligned} \tag{23}$$

All the terms on the right-hand side of the above equation besides the first one, are counter-rotating terms, either becasue they are multiplied by $\Sigma_{b,\mathrm{CRT}}$ or because they are evaluated at twice a phonon frequency apart from the frequency where the equation is evaluated. In general, one can further write an infinite set of linear for this quadrature and its canonical conjugated $\hat{p}_{b,\psi}$, evaluated at frequencies $\omega \pm 2n\omega_b$, where n is a positive integer.

If in addition to the other requirements we further impose that both drives are centered around the magnon/microwave frequency, i.e., if the drive-detuning is zero, then as in the one-tone drive case $\Sigma_b[\omega] = \Sigma_{b,\mathrm{CRT}}[\omega] = 0$. In this particular case:

$$\begin{aligned}\sqrt{2}\chi_b^{-1}[\omega]\hat{x}_{b,\psi}[\omega] = &\sqrt{2\gamma_b}\hat{\xi}_{x_{b,\psi}}[\omega] \\ &- iGe^{-i(2\psi-\varphi)}\hat{\xi}^\dagger_{\mathrm{BA}}[\omega+2\omega_b] + iGe^{i(2\psi-\varphi)}\hat{\xi}_{\mathrm{BA}}[\omega-2\omega_b] \\ &- iGe^{-i(2\psi+\varphi)}\hat{\xi}_{\mathrm{BA}}[\omega+2\omega_b] + iGe^{i(2\psi+\varphi)}\hat{\xi}^\dagger_{\mathrm{BA}}[\omega-2\omega_b].\end{aligned} \tag{24}$$

Since in this situation microwaves and magnons are at resonance, $n_m = n_c$. The noise spectrum of such quadrature is then given by

$$S_{xx,\psi}[\omega] = \int \frac{d\omega'}{2\pi}\langle \hat{x}_{b,\psi}[\omega]\hat{x}_{b,\psi}[\omega']\rangle = S^{(0)}_{xx,\psi}[\omega] + S^{(\mathrm{CRT})}_{xx,\psi}[\omega], \tag{25}$$

where

$$S^{(0)}_{xx,\psi}[\omega] = \gamma_b|\chi_b[\omega]|^2\left(n_b + \frac{1}{2}\right) = \frac{\gamma_b\left(n_b+\frac{1}{2}\right)}{\omega^2 + \frac{\gamma_b^2}{4}}, \tag{26}$$

is the uncoupled noise spectrum, and

$$\begin{aligned}S^{(\mathrm{CRT})}_{xx,\psi}[\omega] = |\chi_b[\omega]|^2G^2\left(n_m+\frac{1}{2}\right)\Bigg[&\mathcal{A}[\omega-2\omega_b]\left(1 - \frac{\chi_b^*[\omega-4\omega_b]e^{4i\psi}}{\chi_b^*[\omega]}\right) \\ &+ \mathcal{A}[\omega+2\omega_b]\left(1 - \frac{\chi_b^*[\omega+4\omega_b]e^{-4i\psi}}{\chi_b^*[\omega]}\right)\Bigg],\end{aligned} \tag{27}$$

where

$$\mathcal{A}[\omega] = |\Xi_m[\omega]|^2(\kappa_m + g^2_{mc}\kappa_c|\chi_c[\omega]|^2). \tag{28}$$

Notice that since the drive detuning $\Delta_c = \Delta_m = 0$ then $\mathcal{A}[\omega] = \mathcal{A}[-\omega]$. Furthermore $\chi_b[\omega] = \chi_b^*[-\omega]$.

In Fig. 3 we compute the effects of the counter-rotating terms in the QND quadrature noise spectrum by evaluating its integral and comparing it with the value for a resonator in thermal equilibrium. We notice that, for the chosen parameters, in the worst case, the corrections introduced by the CRTs does not exceed $4\,10^{-4}I^{(0)}_{xx}$, which is around two orders of magnitude smaller than the same quantity evaluated for the single drive case shown in Fig. 5. In this two-tone case, the CRTs would add a negligible amount of noise when compared to the noise added by quantum backaction in the single-tone case at zero detuning. We also notice that errors introduced by the CRTs are typically an order of magnitude smaller than the error introduced by imperfections on BAE conditions, see section IIIB.

In the case where the detunings do not vanish, the analysis of the effects of counter-rotating terms is more involving. The position quadrature operator is given by Eq. (23), which depends on the phonon operators $\hat{b}^{(\dagger)}[\omega \pm 2\omega_b]$ and $\hat{b}^{(\dagger)}[\omega \pm 4\omega_b]$. As mentioned above, one then has to solve an infinite system of linear equations, which can be truncated at a given order. We postpone such an analysis to a future work, but we expect that, as in the case $\Delta_m = \Delta_c = 0$, the corrections due to discarded counter-rotating terms are small.

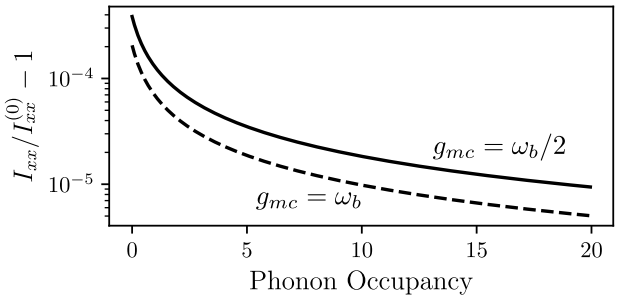

FIG. 3. Ratio between the integral of the noise spectrum of the BAE quadrature including the counter-rotating terms and its value without counter-rotating terms, for both the triple resonance and the dynamical backaction evasion schemes. Parameters as in Table I.

2. *Momentum noise spectral density*

For the case where both drives are not centered around the magnon/microwave frequency, from Eq. (39) we get for the noise spectrum of the momentum quadrature

$$S_{pp}[\omega] = S^{(0)}[\omega] + S_{pp}^{(\mathrm{D})}[\omega] + S_{pp}^{(\mathrm{BA})}[\omega] + S_{pp}^{(\mathrm{DBA})}[\omega]. \tag{29}$$

The terms $S^{(0)}[\omega]$ and $S_{pp}^{(\mathrm{BA})}[\omega]$ are defined in the main text in Eqs.(40) and (42) respectively. The additional contributions are $S_{pp}^{(\mathrm{D})}[\omega]$, a term that comes from the phonon noise and depends on the phonon self-energy, given by

$$S_{pp}^{(\mathrm{D})}[\omega] = \frac{4|\Sigma_b[\omega]|^2}{\omega^2 + \frac{\gamma_b^2}{4}} \left(n_b + \frac{1}{2}\right), \tag{30}$$

while the second backaction noise contribution $S_{pp}^{(\mathrm{DBA})}[\omega]$ is given by

$$S_{pp}^{(\mathrm{DBA})}[\omega] = -\frac{2\sqrt{\gamma_b}\mathrm{Im}[\chi_b[\omega]\Sigma_b[\omega]]}{\omega^2 + \frac{\gamma_b^2}{4}}. \tag{31}$$

3. *Position noise spectrum: deviations from the BAE setup*

Starting with the full solution for $\hat{b}[\omega]$ given in Eq. (15), we drop any term that has an argument containing σ_b and solve the set of equations for $\hat{b}[\omega]$ and $\hat{b}^\dagger[\omega]$. This yields

$$\begin{aligned}\chi_{b,\mathrm{eff}}^{-1}[\omega]\hat{b}[\omega] = {} & ig_+^*\mathcal{B}[\omega]\hat{\xi}_{\mathrm{BA}}[\omega] - ig_-^*\hat{\xi}_{\mathrm{BA}}[\omega+\delta_b] + ig_-\mathcal{B}[\omega]\hat{\xi}_{\mathrm{BA}}^\dagger[\omega] \\ & - ig_+\hat{\xi}_{\mathrm{BA}}^\dagger[\omega+\delta_b] + \sqrt{\gamma_b}\hat{\xi}_b[\omega] + \sqrt{\gamma_b}\mathcal{B}[\omega]\hat{\xi}_b^\dagger[\omega+2\delta_b],\end{aligned} \tag{32}$$

where we have defined the auxiliary function

$$\mathcal{B}[\omega] = \frac{f_2[\omega]}{\chi_b^{-1}[\omega+2\delta_b] + i\Sigma_b^*[-\omega-2\delta_b]}. \tag{33}$$

The effective phonon susceptibility $\chi_{b,\mathrm{eff}}^{-1}[\omega]$ is given by

$$\chi_{b,\mathrm{eff}}^{-1}[\omega] = \chi_b^{-1}[\omega] - i\Sigma_b[\omega] - f_2^*[-\omega-2\delta_b]\mathcal{B}[\omega]. \tag{34}$$

The self-energy term $\Sigma_b[\omega]$ is given in Eq. (17), while the function $f_2[\omega]$ was defined in Eq. (19).

Before proceeding, we define the following functions

$$\begin{aligned}
\chi_{\rm BA}[\omega] &= g_-\chi_{b,\rm eff}[\omega]\mathcal{B}[\omega]e^{-i\psi} - g_+\chi^*_{b,\rm eff}[-\omega]\mathcal{B}^*[-\omega]e^{i\psi},\\
\chi_+[\omega] &= g_+\chi_{b,\rm eff}[\omega],\\
\chi_-[\omega] &= g^*_-\chi_{b,\rm eff}[\omega],\\
\chi_{\mathcal{B}}[\omega] &= \mathcal{B}[\omega]\chi_{b,\rm eff}[\omega],\\
\mathcal{C}^{(1)}[\omega] &= |\Xi_m[\omega]|^2\left[\kappa_m(n_m+1) + g^2_{mc}\kappa_c|\chi_c[\omega]|^2(n_c+1)\right],\\
\mathcal{C}^{(2)}[\omega] &= |\Xi_m[-\omega]|^2\left[\kappa_m n_m + g^2_{mc}\kappa_c|\chi_c[-\omega]|^2 n_c\right].
\end{aligned} \tag{35}$$

The phase ψ is defined as in the BAE case:

$$\psi = \frac{\arg[g_+] - \arg[g_-]}{2}. \tag{36}$$

We can then calculate the position noise spectrum

$$S_{xx}[\omega] = \int \frac{d\omega'}{2\pi}\langle \hat{x}_{b,\psi}[\omega]\hat{x}_{b,\psi}[\omega']\rangle = S^{(\rm D)}_{xx}[\omega] + S^{(\rm BA)}_{xx}[\omega]. \tag{37}$$

As in the previously studied cases, the first term contains contributions due to dynamical backaction, and is given by

$$\begin{aligned}
S^{(\rm D)}_{xx}[\omega] = &\left[|\chi_{b,\rm eff}[\omega]|^2 + |\chi_{\mathcal{B}}[-\omega]|^2 + \chi_{b,\rm eff}[\omega]\chi_{\mathcal{B}}[-\omega-2\delta_b]e^{-2i\psi} + \chi^*_{b,\rm eff}[\omega-2\delta_b]\chi^*_{\mathcal{B}}[-\omega]e^{2i\psi}\right]\frac{\gamma_b(n_b+1)}{2}\\
&+ \left[|\chi_{b,\rm eff}[-\omega]|^2 + |\chi_{\mathcal{B}}[\omega]|^2 + \chi^*_{b,\rm eff}[-\omega]\chi^*_{\mathcal{B}}[\omega-2\delta_b]e^{2i\psi} + \chi_{b,\rm eff}[-\omega-2\delta_b]\chi_{\mathcal{B}}[\omega]e^{-2i\psi}\right]\frac{\gamma_b n_b}{2},
\end{aligned} \tag{38}$$

The quantum backaction term $S^{(\rm BA)}_{xx}[\omega]$ is given explicitly by

$$\begin{aligned}
S^{(\rm BA)}_{xx}[\omega] = &\left[|\chi_{\rm BA}[-\omega]|^2 + \chi^*_{\rm BA}[-\omega]\chi^*_-[\omega-\delta_b]e^{i\psi} - \chi^*_{\rm BA}[-\omega]\chi_+[-\omega-\delta_b]e^{-i\psi}\right]\frac{\mathcal{C}^{(1)}[\omega]}{2}\\
&+ \left[|\chi_{\rm BA}[\omega]|^2 + \chi_{\rm BA}[\omega]\chi_-[-\omega-\delta_b]e^{-i\psi} - \chi_{\rm BA}[\omega]\chi^*_+[\omega-\delta_b]e^{i\psi}\right]\frac{\mathcal{C}^{(2)}[\omega]}{2}\\
&+ \left[|\chi_-[\omega]|^2 + \chi_-[\omega]\chi_{\rm BA}[-\omega-\delta_b]e^{-i\psi} - \chi_-[\omega]\chi_+[-\omega-2\delta_b]e^{-2i\psi}\right]\frac{\mathcal{C}^{(1)}(\omega+\delta_b)}{2}\\
&+ \left[|\chi_-[-\omega]|^2 + \chi^*_-[-\omega]\chi^*_{\rm BA}[\omega-\delta_b]e^{i\psi} - \chi^*_-[-\omega]\chi^*_+[\omega-2\delta_b]e^{2i\psi}\right]\frac{\mathcal{C}^{(2)}[\omega-\delta_b]}{2}\\
&+ \left[|\chi_+[-\omega]|^2 - \chi^*_+[-\omega]\chi_{\rm BA}[-\omega+\delta_b]e^{i\psi} - \chi^*_+[-\omega]\chi^*_-[\omega-2\delta_b]e^{2i\psi}\right]\frac{\mathcal{C}^{(1)}[\omega-\delta_b]}{2}\\
&+ \left[|\chi_+[\omega]|^2 - \chi_+[\omega]\chi^*_{\rm BA}[\omega+\delta_b]e^{-i\psi} - \chi_+[\omega]\chi_-[-\omega-2\delta_b]e^{-2i\psi}\right]\frac{\mathcal{C}^{(2)}[\omega+\delta_b]}{2}.
\end{aligned} \tag{39}$$

One can check that under the BAE conditions $\delta_b = 0$ and $|g_+| = |g_-| = G$, each term in brackets in the above expression vanishes, and those in Eq. (38) simplify to $|\chi_b[\omega]|^2$.

E. Output microwave spectrum

Here we show the formulas not displayed in the main text for the output microwave spectrum. We consider exclusively the case where the BAE conditions are met. From the Heisenberg-Langevin equations, we obtain the following solution for the microwave operator as a function of the noises and the BAE phonon quadrature

$$\chi_c^{-1}[\omega]\hat{c}[\omega] = -\sqrt{2}Gg_{mc}\Xi_m[\omega]e^{i\phi}\hat{x}_{b,\psi}[\omega] - ig_{mc}\hat{\xi}_{\rm BA}[\omega] + \sqrt{\kappa_c}\hat{\xi}_c[\omega]. \tag{40}$$

Recall that the "backaction" noise term $\hat{\xi}_{\rm BA}[\omega]$ has a component $\hat{\xi}_c[\omega]$, see Eq. (16). We now consider the standard input-output relation for the reflection of the microwave mode and assume that the only source of input noise is thermal, such that

$$\hat{c}_{\rm out}[\omega] = \hat{\xi}_c[\omega] - \sqrt{\kappa_c}\hat{c}[\omega]. \tag{41}$$

We then compute the output quadrature

$$\begin{aligned}\hat{x}_{\mathrm{out},\theta}[\omega] &= \frac{e^{i\theta}\hat{c}^\dagger_{\mathrm{out}}[\omega] + e^{-i\theta}\hat{c}_{\mathrm{out}}[\omega]}{\sqrt{2}} \\ &= \mathcal{G}_{x,\theta}[\omega]\hat{x}_{b,\psi}[\omega] + \mathbb{A}_{m;\theta}[\omega]\hat{\xi}_m[\omega] + \mathbb{A}_{c;\theta}[\omega]\hat{\xi}_c[\omega] \\ &\quad + \mathbb{A}^*_{m;\theta}[-\omega]\hat{\xi}^\dagger_m[\omega] + \mathbb{A}^*_{c;\theta}[-\omega]\hat{\xi}^\dagger_c[\omega].\end{aligned} \tag{42}$$

The coefficients appearing in the above expression are

$$\begin{aligned}\mathcal{G}_{x,\theta}[\omega] &= \sqrt{\kappa_c}Gg_{mc}\left[\chi_c[\omega]\Xi_m[\omega]e^{i(\phi-\theta)} + \chi^*_c[-\omega]\Xi^*_m[-\omega]e^{-i(\phi-\theta)}\right], \\ \mathbb{A}_{m;\theta}[\omega] &= ig_{mc}\sqrt{\frac{\kappa_c\kappa_m}{2}}\chi_c[\omega]\Xi_m[\omega]e^{-i\theta}, \\ \mathbb{A}_{c;\theta}[\omega] &= \left(1 - \kappa_c\frac{\chi_c[\omega]}{\chi_m[\omega]}\Xi_m[\omega]\right)\frac{e^{-i\theta}}{\sqrt{2}}.\end{aligned} \tag{43}$$

The correlation noise spectrum between two of such quadratures is given by

$$S_{\theta\theta'}[\omega] = \int \frac{d\omega'}{2\pi}\langle \hat{x}_{\mathrm{out},\theta}[\omega]\hat{x}_{\mathrm{out},\theta'}[\omega']\rangle, \tag{44}$$

and then the self-correlation, obtained for $\theta = \theta'$ reads explicitly

$$\begin{aligned}S_{\theta\theta}[\omega] &= |\mathcal{G}_{x,\theta}[\omega]|^2 S^{(0)}[\omega] \\ &\quad + |\mathbb{A}_{m,\theta}[\omega]|^2(n_m+1) + |\mathbb{A}_{m,\theta}[-\omega]|^2 n_m \\ &\quad + |\mathbb{A}_{c,\theta}[\omega]|^2(n_c+1) + |\mathbb{A}_{c,\theta}[-\omega]|^2 n_c.\end{aligned} \tag{45}$$

In order to obtain the noise added to the measurement of $S^{(0)}[\omega]$ we write

$$S_{\theta\theta}[\omega] = |\mathcal{G}_{x,\theta}[\omega]|^2\left[S^{(0)}[\omega] + S_{\mathrm{imp}}[\omega]\right], \tag{46}$$

where

$$S_{\mathrm{imp}}[\omega] = \frac{1}{|\mathcal{G}_{x,\theta}[\omega]|^2}\left[|\mathbb{A}_{m,\theta}[\omega]|^2(n_m+1) + |\mathbb{A}_{m,\theta}[-\omega]|^2 n_m + |\mathbb{A}_{c,\theta}[\omega]|^2(n_c+1) + |\mathbb{A}_{c,\theta}[-\omega]|^2 n_c\right]. \tag{47}$$

We notice now that, at $\omega = 0$

$$\begin{aligned}S_{\theta\theta}(0) &= |\mathcal{G}_{x,\theta}(0)|^2\left[S^{(0)}(0) + S_{\mathrm{imp}}(0)\right] \\ &= |\mathbb{A}_{x,\theta}(0)|^2\frac{2}{\gamma_b}\left[2n_b + 1 + \frac{\gamma_b}{2}S^{(0)}_{\mathrm{imp}}(0)\right].\end{aligned} \tag{48}$$

We then define the added quanta to the measurement due to the imprecision noise as

$$n_{\mathrm{imp},\theta} = \frac{\gamma_b}{4}S_{\mathrm{imp},\theta}(0). \tag{49}$$

Since for frequencies ω close to zero we have $S_{\mathrm{imp}}[\omega] \approx S_{\mathrm{imp}}(0)$, we can write

$$S_{\theta\theta}[\omega] = |\mathcal{G}_{x,\theta}[\omega]|^2\left[S^{(0)}[\omega] + \frac{4n_{\mathrm{imp},\theta}}{\gamma_b}\right]. \tag{50}$$

We note that, for schemes that break the BAE conditions, the phonon quadrature will include a backaction noise term, which then correlates with the imprecision noise.

The imprecision noise for a given angle θ is below the standard quantum limit provided that $n_{\mathrm{imp},\theta} < 1/2$. For magnons at resonance with microwaves, the bath occupancy of such modes $n_{m,c}$ has to satisfy

$$n_{m,c} < \frac{|\mathcal{G}_{x,\theta}[0]|^2}{\gamma_b(|\mathbb{A}_{m,\theta}[0]|^2) + |\mathbb{A}_{c,\theta}[0]|^2)} - \frac{1}{2}. \tag{51}$$

The maximum occupancy of the magnon/microwave baths for beating the SQL depends on the gain factor $|\mathcal{G}_{x,\theta}[0]|^2$, which scales linearly with the drive power. In general, strong drive powers allow to beat the SQL at higher bath occupancies, while smaller phonon decays also allow higher $n_{c,m}$. We should nevertheless notice that the typical temperature required for having a negligible occupancy of the magnon/microwave bath is of a few hundreds of mK, a condition attainable routinely in cavity magnonics experiments.

1. Brief comparison with the single tone drive case

We can obtain the output noise spectrum for the case of a single tone drive by following the same procedure presented above for the single-tone drive case using the frequency domain Heisenberg-Langevin equation shown in Sec. II. The result for the output noise spectrum $S_{\theta\theta}[\omega]$, define in the same way as in the backaction evasion framework, is given in this case by

$$S_{\theta\theta}[\omega] = |\mathcal{G}_{x,\theta}[\omega]|^2 \left[S_{xx}^{(\mathrm{D})}[\omega] + S_{xx}^{(\mathrm{BA})}[\omega] + S_{\mathrm{imp}}[\omega] + S_{\mathrm{corr}}[\omega] \right]. \tag{52}$$

In the above expression $S_{xx}^{(\mathrm{D})}$ and $S_{xx}^{(\mathrm{BA})}$ are given by Eqs. (24) and (25) respectively. The gain term $\mathcal{G}_{x,\theta}[\omega]$ is given as in Eq. (43) with $G \to |g_{mb}|$ and $\phi = \arg[g_{mb}]$. The imprecision noise $S_{\mathrm{imp}}[\omega]$ is given by (47). Finally the correlation noise $S_{\mathrm{corr}}[\omega]$ comes from correlations between the backaction noise terms appearing in the solution for $\hat{x}_b[\omega]$ and the imprecision noise terms.

Comparing this expression with what was obtained in the backaction evasion case we notice the presence of bakcation and correlation noises as well as a change in the bare phonon noise due to dynamical backaction, as described by $S_{xx}^{(\mathrm{D})}$. In analogy with the previous case, we have the number of added quanta to the measurement given by

$$n_{\mathrm{add}} = n_{\mathrm{imp}} + n_{\mathrm{BA}} + n_{\mathrm{corr}}, \tag{53}$$

where

$$\begin{aligned} n_{\mathrm{imp}} &= \frac{\tilde{\gamma}_b}{4} S_{\mathrm{imp}}[\omega_b], \\ n_{\mathrm{BA}} &= \frac{\tilde{\gamma}_b}{4} S_{xx}^{(\mathrm{BA})}[\omega_b], \\ n_{\mathrm{corr}} &= \frac{\tilde{\gamma}_b}{4} S_{\mathrm{corr}}[\omega_b]. \end{aligned} \tag{54}$$

As in typical linear systems, backaction noise prevents the measurement to go bellow the standard quantum limit $n_{\mathrm{add}} = 1/2$ [2].

---

[1] V. B. Braginsky, Y. I. Vorontsov, and K. S. Thorne, Quantum nondemolition measurements, Science **209**, 547 (1980).

[2] A. A. Clerk, M. H. Devoret, S. M. Girvin, F. Marquardt, and R. J. Schoelkopf, Introduction to quantum noise, measurement, and amplification, Rev. Mod. Phys. **82**, 1155 (2010).

[3] A. A. Clerk, F. Marquardt, and K. Jacobs, Back-action evasion and squeezing of a mechanical resonator using a cavity detector, New J. Phys. **10**, 095010 (2008).

[4] M. J. Woolley and A. A. Clerk, Two-mode back-action-evading measurements in cavity optomechanics, Phys. Rev. A **87**, 063846 (2013).

[5] M. Aspelmeyer, T. J. Kippenberg, and F. Marquardt, Cavity optomechanics, Rev. Mod. Phys. **86**, 1391 (2014).

[6] Y. Yanay and A. A. Clerk, Shelving-style qnd phonon-number detection in quantum optomechanics, New Journal of Physics **19**, 033014 (2017).

[7] B. D. Hauer, A. Metelmann, and J. P. Davis, Phonon quantum nondemolition measurements in nonlinearly coupled optomechanical cavities, Phys. Rev. A **98**, 043804 (2018).

[8] I. Shomroni, L. Qiu, D. Malz, A. Nunnenkamp, and T. J. Kippenberg, Optical backaction-evading measurement of a mechanical oscillator, Nat. Commun. **10**, 1 (2019).

[9] J. Hertzberg, T. Rocheleau, T. Ndukum, M. Savva, A. A. Clerk, and K. Schwab, Back-action-evading measurements of nanomechanical motion, Nat. Phys. **6**, 213 (2010).

[10] F. Lecocq, J. B. Clark, R. W. Simmonds, J. Aumentado, and J. D. Teufel, Quantum nondemolition measurement of a nonclassical state of a massive object, Phys. Rev. X **5**, 041037 (2015).

[11] C. Ockeloen-Korppi, E. Damskägg, J.-M. Pirkkalainen, A. Clerk, M. Woolley, and M. Sillanpää, Quantum backaction evading measurement of collective mechanical modes, Phys. Rev. Lett. **117**, 140401 (2016).

[12] C. B. Møller, R. A. Thomas, G. Vasilakis, E. Zeuthen, Y. Tsaturyan, M. Balabas, K. Jensen, A. Schliesser, K. Hammerer, and E. S. Polzik, Quantum back-action-evading measurement of motion in a negative mass reference frame, Nature **547**, 191 (2017).

[13] E. Altuntaş and I. B. Spielman, Quantum back-action limits in dispersively measured bose-einstein condensates, Communications Physics **6**, 66 (2023).

[14] J. Gambetta, A. Blais, D. I. Schuster, A. Wallraff, L. Frunzio, J. Majer, M. H. Devoret, S. M. Girvin, and R. J. Schoelkopf, Qubit-photon interactions in a cavity: Measurement-induced dephasing and number splitting, Phys. Rev. A **74**, 042318 (2006).

[15] X. Zhang, C.-L. Zou, L. Jiang, and H. X. Tang, Cavity magnomechanics, Sci. Adv. **2**, e1501286 (2016).

[16] B. Z. Rameshti, S. Viola Kusminskiy, J. A. Haigh, K. Usami, D. Lachance-Quirion, Y. Nakamura, C.-M. Hu, H. X. Tang, G. E. Bauer, and Y. M. Blanter, Cavity magnonics, Phys. Rep. **979**, 1 (2022).

[17] R. LeCraw, E. Spencer, and E. Gordon, Extremely low loss acoustic resonance in single-crystal garnet spheres, Physical Review Letters **6**, 620 (1961).

[18] E. G. Spencer and R. LeCraw, Magnetoacoustic resonance in yttrium iron garnet, Physical Review Letters **1**, 241 (1958).

[19] C. Gonzalez-Ballestero, D. Hümmer, J. Gieseler, and O. Romero-Isart, Theory of quantum acoustomagnonics and acoustomechanics with a micromagnet, Phys. Rev. B **101**, 125404 (2020).

[20] J. Li, S.-Y. Zhu, and G. Agarwal, Magnon-photon-phonon entanglement in cavity magnomechanics, Phys. Rev. Lett. **121**, 203601 (2018).

[21] J. Li and S. Gröblacher, Entangling the vibrational modes of two massive ferromagnetic spheres using cavity magnomechanics, Quantum Sci. Tech. **6**, 024005 (2021).

[22] Z.-Y. Fan, L. Qiu, S. Gröblacher, and J. Li, Microwave-optics entanglement via cavity optomagnomechanics, Laser & Photonics Reviews **n/a**, 2200866 (2022).

[23] J. Li, Y.-P. Wang, J.-Q. You, and S.-Y. Zhu, Squeezing microwaves by magnetostriction, National Science Review **10**, nwac247 (2022).

[24] M.-S. Ding, L. Zheng, Y. Shi, and Y.-J. Liu, Magnon squeezing enhanced entanglement in a cavity magnomechanical system, J. Opt. Soc. Am. B **39**, 2665 (2022).

[25] C. A. Potts, V. A. S. V. Bittencourt, S. Viola Kusminskiy, and J. P. Davis, Magnon-phonon quantum correlation thermometry, Phys. Rev. Appl. **13**, 064001 (2020).

[26] F. Engelhardt, V. Bittencourt, H. Huebl, O. Klein, and S. V. Kusminskiy, Optimal broadband frequency conversion via a magnetomechanical transducer, Phys. Rev. Appl. **18**, 044059 (2022).

[27] C. A. Potts, E. Varga, V. A. S. V. Bittencourt, S. Viola Kusminskiy, and J. P. Davis, Dynamical backaction magnomechanics, Phys. Rev. X **11**, 031053 (2021).

[28] C. A. Potts, Y. Huang, V. A. S. V. Bittencourt, S. Viola Kusminskiy, and J. P. Davis, Dynamical backaction evading magnomechanics, Phys. Rev. B **107**, L140405 (2023).

[29] M. Amazioug, B. Teklu, and M. Asjad, Enhancement of magnon–photon–phonon entanglement in a cavity magnomechanics with coherent feedback loop, Scientific Reports **13**, 3833 (2023).

[30] W. Zhang, D.-Y. Wang, C.-H. Bai, T. Wang, S. Zhang, and H.-F. Wang, Generation and transfer of squeezed states in a cavity magnomechanical system by two-tone microwave fields, Opt. Express **29**, 11773 (2021).

[31] H. Qian, X. Zuo, Z.-Y. Fan, J. Cheng, and J. Li, Strong squeezing of microwave output fields via reservoir-engineered cavity magnomechanics, Phys. Rev. A **109**, 013704 (2024).

[32] Z.-X. Liu, J. Peng, and H. Xiong, Generation of magnonic frequency combs via a two-tone microwave drive, Phys. Rev. A **107**, 053708 (2023).

[33] V. A. S. V. Bittencourt, C. A. Potts, Y. Huang, J. P. Davis, and S. Viola Kusminskiy, Magnomechanical backaction corrections due to coupling to higher-order walker modes and kerr nonlinearities, Phys. Rev. B **107**, 144411 (2023).

[34] D. D. Stancil and A. Prabhakar, *Spin Waves: Theory and Applications* (Springer, New York, 2010).

[35] H. Huebl, C. W. Zollitsch, J. Lotze, F. Hocke, M. Greifenstein, A. Marx, R. Gross, and S. T. Goennenwein, High cooperativity in coupled microwave resonator ferrimagnetic insulator hybrids, Phys. Rev. Lett. **111**, 127003 (2013).

[36] Y. Tabuchi, S. Ishino, A. Noguchi, T. Ishikawa, R. Yamazaki, K. Usami, and Y. Nakamura, Coherent coupling between a ferromagnetic magnon and a superconducting qubit, Science **349**, 405 (2015).

[37] E. Callen, Magnetostriction, J. Appl. Phys. **39**, 519 (1968).

[38] X. Zhang, C.-L. Zou, L. Jiang, and H. X. Tang, Strongly coupled magnons and cavity microwave photons, Phys. Rev. Lett. **113**, 156401 (2014).

[39] C. A. Potts and J. P. Davis, Strong magnon–photon coupling within a tunable cryogenic microwave cavity, Appl. Phys. Lett. **116**, 263503 (2020).

[40] A. Eringen and E. Suhubi, *Elastodynamics: Linear Theory* (Academic Press, New York, 1975).

[41] In the following we use the Fourier transform (for $\hat{o} = \hat{c}, \hat{m}, \hat{b}$):

$$\hat{o}(t) = \int_{-\infty}^{\infty} \frac{d\omega}{2\pi} e^{-i\omega t} \hat{o}[\omega].$$

Notice that

$$\hat{o}^\dagger[\omega] = \int dt e^{i\omega t} \hat{o}^\dagger(t) = (\hat{o}[-\omega])^\dagger.$$

.

[42] D. Lachance-Quirion, Y. Tabuchi, A. Gloppe, K. Usami, and Y. Nakamura, Hybrid quantum systems based on magnonics, Appl. Phys. Express **12**, 070101 (2019).